Computers in Industry 179 (2026) 104495

Contents lists available at ScienceDirect

Computers in Industry

journal homepage: www.sciencedirect.com/journal/computers-in-industry

Automated uncrewed aerial system data acquisition for rebar layout inspection in the construction industry

Mahsa Sanei [a], Ali Mohammadkhorasani [a], G. Matthew Fricke [b], Fernando Moreu [a,*]

[a] Department of Civil, Construction, and Environmental Engineering, University of New Mexico, United States
[b] Department of Computer Science, University of New Mexico, United States

ARTICLE INFO

Keywords:
RGBD camera
3D scanning
Uncrewed Aerial System
Image processing
Rebar geometric information

ABSTRACT

Conducting visual inspections is important in determining the quality of construction. While visual assessment has merits, it is time consuming, subjective and can be unsafe for the inspectors. Many studies have explored remote sensing for automated rebar inspection and quality control; however, there has been limited focus on applying these technologies in the construction industry, especially with Uncrewed Aerial Systems (UAS). We developed a rebar inspection system that uses a low-cost Red-Green-Blue-Depth-equipped UAS to automate data acquisition and apply computer vision techniques. The system was tested with a horizontal rebar mat in a controlled setting. This experiment investigated three different distances and UAS flight patterns to find the best quality data for industry applications. UAS scans of the horizontal rebar mat at approximately three feet with constant velocity and direction, produced the highest accuracy and average error of 2.58 mm. The findings from the controlled environment were then adapted to scan vertical rebar at an active construction site. Results indicated the proposed method can obtain an average rebar spacing measurement error of 0.44 mm. This development enhances quality control, assurance processes, and it simplifies rebar inspection by eliminating the necessity for manual inspections at elevated rebar cage positions.

1. Introduction

Ensuring appropriate rebar spacing in reinforced concrete (RC) structures is essential. Efficient rebar spacing control can enhance the structural quality and strength by preventing crack formation and excessive deflection in concrete structures (Pantazopoulou and Papoulia, 2001), which increases the lifelong service of RC structures (Masoumi et al., 2013). One of the inspection tasks prior to pouring concrete is to evaluate the accuracy of rebar placement based on the structural design specifications (Ma et al., 2022). The current approach for rebar placement quality control relies on inspectors visually checking each bar. This requirement means that inspectors must thoroughly observe rebar positions to ensure that construction complies with the design drawings and building codes applicable to the project (Han et al., 2013). However, this method presents several challenges in the construction field. Traditional visual inspections are often characterized by their lengthy duration, demanding labor requirements, and relatively high costs (Washer and Chang, 2009). Additionally, the act of walking over the rebar during inspections poses a risk to the inspector and the structural integrity of the building due to potential deformation of the bars (Sanford et al., 1999). Therefore, automating data acquisition and utilizing computer-aided analysis can benefit quality control in the RC construction industry.

Using automated inspection systems can reduce evaluation time, cost, and improve inspection quality. Recent advancements in technologies have encouraged researchers to explore automation in RC construction industry involving computer systems (Ploennigs et al., 2014; Zhang et al., 2018). For example, Asadi et al. (2018) developed a mobile data acquisition system that uses different vision-based elements to monitor the construction site in real time with low computational usage in order to improve the overall inspection quality control process. The inspection operator could then focus on making informed decisions based on the data collected by the robotic system, so this automated system does not replace the human with a robot but keeps them in the loop for decision making (Villani et al., 2018). Involving stakeholders and considering their knowledge and preferences in the decision-making process can lead to more sustainable decisions in the built environment (Hill et al., 2023). As the nature of rebar inspection is a time-consuming, demanding task for inspectors, computers and new technologies could be adopted in the rebar inspection industry, and in this way higher

* Correspondence to: Centennial Engineering Center3051, 210 University Blvd, NE, MSC01 1070, Albuquerque, NM 87131, United States.
E-mail address: fmoreu@unm.edu (F. Moreu).

https://doi.org/10.1016/j.compind.2026.104495
Received 24 June 2024; Received in revised form 5 September 2025; Accepted 18 May 2026
Available online 28 May 2026

standards of construction quality could be attained safely and consistently. A human inspector can then make informed decisions faster with the data collected and analyzed by an automated system.

So far, research in the area of automating rebar inspection in the RC construction industry has been conducted in laboratory settings rather than real construction sites, which present unique challenges. This study aims to develop a system that integrates a depth-color camera and a drone to automate rebar data acquisition. An integration of edge detection and transformation is proposed for detecting the individual bars from the point cloud data collected by the camera-drone system. This integration allows for precise detection of rebar edges and alignment, even in noisy or low-contrast images commonly found in real construction sites. It also adapts well to different rebar arrangements, making it a scalable and reliable solution for improving quality control in construction. The system then provides numerical and color representations of rebar spacing error of construction from the design drawings, making it easier for inspectors and decision-makers to interpret the results in a real construction environment. To optimize data acquisition, various flight patterns and distances were tested to determine the optimal accuracy for analysis. The following section provides an overview of the current state of machine-enabled technologies used in construction for rebar placement inspection, as well as the application of drones in structural inspections. The methodology section describes the approach used to estimate rebar spacing. The next section discusses experiments in controlled environment with three different flight patterns and distances to assess accuracy under varying conditions. Based on insights from the controlled experiments, the next section describes the validation of the algorithm in a real construction setting. Finally, the study discusses the recommendations and limitations of the developed system for rebar inspection, with key findings highlighted in the conclusion.

2. Computers and automation of rebar inspection

Computers and automation are changing the way rebar inspections are done in the construction industry. This study focuses on two types of automation: collecting and analyzing rebar data and utilizing UASs to quickly access different areas of construction sites. These technologies enhance safety by reducing the need for inspectors to physically go to inaccessible areas, improving the precision and speed of inspections.

2.1. Rebar geometric information quantification state-of-the-art

Over the past few years, the automated inspection of RC elements has been investigated using a variety of technologies, including Augmented Reality (Mohammadkhorasani et al., 2023), 2D cameras, 3D laser scanners, and other camera-based methods. In the field of noncontact inspection of rebar, the most commonly used sensing technologies are Light Detection and Ranging (LiDAR) and depth cameras (Narasimhan and Wang, 2020). The summary of the related research in automated rebar inspection is discussed in Table 1.

The current state-of-the-art methods for automatic rebar inspection, while advanced in terms of cost-effectiveness and accuracy, show several gaps. Many methods depend on high-quality image or scan data, precise parameter settings, and stable conditions, limiting their practicality in real-world scenarios. Several approaches are limited to specific conditions or components such as laboratory setup, horizontal components, and therefore lack generalizability. Moreover, methods limited to laboratory settings that need control points are impractical for different types of RC structures. Additionally, field application has only been done in one study (Yuan et al., 2023), highlighting a significant gap in real-world validation. Bridging these gaps requires developing an automatic system of data acquisition and analysis at real construction sites that maintains high accuracy for rebar inspection.

Therefore, in this study, a low-cost data acquisition system is developed using a Red-Green-Blue-Depth (RGBD) camera combined with a computer vision technique. This approach eliminates the need for multiple high-density images and is effective for inspecting both horizontal and vertical rebar in laboratory settings and real construction sites. The next section discusses the applicability of using UAS equipped with RGBD cameras to facilitate data collection in real construction sites, thereby reducing the time required for data collection and improving access to different parts of the structure.

2.2. Application of UAS in inspection of structure state-of-the-art

UAS-based remote sensing technology has recently emerged as a practical solution to address some of the issues during inspection, such as risk to the inspector and the time-consuming nature of data collection (Jordan et al., 2018). UASs are now much more accessible to the government and academic institutions due to their lower cost. A notable advantage of UASs is their capacity to provide access to the inaccessible or dangerous areas of a structure, allowing the scanning system to collect a more extensive array of data points from a closer point of damaged surfaces. This unmanned strategy also mitigates dangers to inspectors (Metni and Hamel, 2007). Table 2 shows a comparison between human and UAS in inspection task. In the past few decades, many researchers have worked on studies emphasizing the capabilities of UAS equipped with different type of tools, for example, LiDAR (Wood et al., 2022; Gaspari et al., 2022; Schwind et al., 2018; Jung et al., 2019; Faria et al., 2019), and other sensors used for the inspection and monitoring of structures.

Both humans and UAS have pros and cons, therefore the choice of which one to use for inspection generally depends on the nature of the inspection, limitations of the site, cost, and the accuracy needed for inspection. Inspecting rebar in areas that are unsafe or difficult to access, such as high-rise buildings and bridges, is challenging. UAS could potentially be a safer and more efficient alternative by making some adjustments for rebar inspection applications. For example, UAS can be scheduled to operate under better conditions during clear weather and non-working hours. Nowadays, UAS are capable of following preprogrammed flight paths without the need for direct pilot control. In rebar inspections, UAS typically have enough battery life to scan an entire structure. Unlike humans, who may experience fatigue or variations in inspection, UAS can provide more accurate, repeatable measurements across large areas. Human inspectors often randomly select the rebar and manually perform the measurements, which is impractical. However, UAS can scan the entire site in a single flight, ensuring no critical details are overlooked. While human expertise is still needed for interpreting results, UAS enhance safety and efficiency in rebar inspections.

Marchisotti and Zappa (2022) discussed UAS-based 3D investigation of defects and damages in concrete structures using a variety of available methods and sensors. The use of ToF sensors, drone-based inspection images, and integration with deep learning and image processing techniques have shown promising results in detecting and measuring defects in concrete structures. Eschmann et al. (2012) employed micro-aircraft and high-definition digital cameras to perform a building inspection and monitoring process based on digital imaging. The outcome was a computerized 2D facade reconstruction using images with resolution that can automatically detect the crack patterns. Roca et al. (2014) presented a system for point cloud data creation using LiDAR-equipped Unmanned Aerial Vehicle (UAV) to generate a 3D model of a building using BIM. Nasrollahi et al. (2018) constructed a platform to use low-cost 2D LiDAR-equipped UAV for inspection. They used a servo motor to be able to rotate the 2D data and convert it to 3D. They tested their system on fixed mode in an indoor space. Santos et al. (2022) used combination of deep learning methods, such as CNN, for exposed steel rebar detection in RC structures. They used UAS equipped with AI platforms, and 3D cameras for data collection, processing and transmission optimization.

There are also a few studies that used camera-equipped UAS for rebar

Table 1
Automated rebar inspection state of the art.

	Study	Rebar?	Tools	Method	Field tested?	Accuracy	Fully automated?	Advantages	Limitations
Camera-Based	Han et al., (2013)	S	Digital camera	SfM+MVS	No	~0.6 cm	No	Low-cost, handles occlusion	Manual registration, image-sensitive
	Zhang et al., (2018)	D, S, Q	Smartphone	Sub-pixel ML + Stitching	No	0.04 mm (abs.)	Yes	High precision, real-time, mobile	Stable setup required
	Golparvar-Fard et al., (2012)	S	Digital camera	Image-based 3D + pattern recognition	No	~0.4 mm (≥130 images/9.3 m^2)	No	BIM integration, automated mapping	Needs high image coverage
	Qureshi et al., (2024)	S, D, L, Q	Smartphone	Photogrammetry + AI	No	S: 2.56%, D: 90%, L: 0.72%, Q: 100%	Yes	Multi-parameter inspection, cost-effective	Image resolution dependency
	Wang et al., (2024)	Q	Digital camera	Faster R-CNN/YOLO	Yes	AP50 up to 94.9%	Yes	Large dataset, public release	Limited environmental diversity, lack of variation; No spacing /diameter detection
	Chang et al., (2024)	D, S	GoPro	SfM + Mask R-CNN	Yes	S: 1.61 mm spacing MAE	Yes	handles complex layouts	Small-diameter performance drop; sensitive to image scale; training needed
LiDAR/Laser Scanner	Wang et al., (2017)	S	TLS	Model fitting + OCC	No	0.9 mm	No	High accuracy, robust filtering	Occlusion-sensitive, training needed
	Kim et al., (2020)	S, C, F	TLS	PCA, RANSAC, DBSCAN	No	S: 2.15 mm, F: 2.52 mm, C: 2.18 mm	No	Automated DQA pre-concrete	Small-scale only; affected by scan density, occlusion
	Kim et al., (2021)	D, S	TLS	Density-based ML	No	D: 97.2% (large diameters), S ~2.2 mm	No	High large-bar accuracy	Poor small-diameter accuracy, needs ≥ 10 pts/cm^2 scan density
	Nishio et al., (2017)	S	3D laser scanner	Point cloud thinning + vector	No	Qualitative only	No	Robust core wire detection, handles loops	Needs precise parameter tuning, discontinuities at intersection
	Owerko and Owerko, (2021)	S	3D laser scanner	Photogrammetry + HDS	Yes	1.4 mm (photo), 1–4 mm (TLS)	No	Low-cost, high accuracy	Photogrammetry fails for web rebar; slow (48 h)
	Yuan, Smith, et al., (2021)	S	Handheld LiDAR	Slicing algorithm	No	0.32–0.80 in	No	Objective, quick (~30 s scan)	Noise-sensitive
	Yuan et al., (2023)	S, F, C	Mobile LiDAR	Slicing algorithms	Yes	~0.2–0.5 in	No	Full bridge inspection in 1 hr	Manual cropping/denoising
	Wang et al., (2025)	S, L	Spinning 2D LiDAR	RANSAC + DBSCAN + GMM	No	S: 4.58 mm, L: 4.15 mm	Yes	Cost-effective, portable, 5 min scan	Sensitive to scan angle, single-view occlusion
RGBD-based	Yuan, Moreu, et al., (2021)	S, C	RGBD camera	Slicing algorithm	No	S: 1.10 in; C: 0.38 in	No	Cost-effective, fast	Manual segmentation
	The present study	S	RGBD camera	Sobel edge detection + Hough transformation	Yes	0.44 mm	No	Low-cost, safe for elevated scans	Limited range, flight-sensitive

S=Spacing, D=Diameter, L=Length, Q=Quantity, C=Cover, F=Formwork

Table 2
Inspection method comparison.

Inspection Method	Strengths	Limitations
UAS (Nishio et al. 2017; Yuan et al. 2023; Yuan, Smith, et al. 2021; Wang et al. 2025)	• Equipped with high-resolution cameras for detailed inspection. • Has the ability to reach inaccessible or dangerous areas without risking human safety. • Easily adaptable for various types of inspections by changing sensors or cameras. • Can transmit real-time data to inspectors and experts off-site. • Can operate continuously without fatigue.	• Limited to the capabilities and safety measures of the UAS itself. • Requires initial setup and equipment costs. • Needs pilot. • Limited Time of Flight (ToF). • Limited flying area. • Inapplicable in the harsh weathering conditions. • Permission needed. • Magnetic interference, shadowing effects.
Human Inspectors (Yuan, Moreu, et al., 2021; Metni and Hamel, 2007; Jordan et al., 2018)	• Experienced human eyes can detect subtle structural issues. • Can access hard-to-reach areas manually (e.g., confined spaces). • Can adapt to changing conditions or issues.	• Inspection of hazardous or high-risk areas can endanger human inspectors. • Visual inspection can be time-consuming. • Inspection results can vary due to individual judgment and bias. • Hiring and training skilled inspectors can be costly.

count and inspection. Sanei et al. (2023) tested the RGBD-equipped UAS system on a simulated bridge deck and small rebar specimen to see the operation and performance of their system in different settings and with different UAS movements. Wang et al. (2023) used UAS to create a model for counting the bars with six different deep learning algorithms, through which they achieved the best result with faster R-CNN model. Machine learning techniques offer a competitive advantage with respect to detection accuracy for scenarios with low point cloud densities. Nevertheless, compared to computer vision approaches, they frequently need longer processing times. This is mostly because tasks like data pre-processing, training, and validation are required. Additionally, access to a large number of labeled data is usually necessary to achieve high accuracy with these methods Braun and Borrmann (2019). The complexity associated with utilizing machine learning algorithms, providing labeled data, and employing UASs in the field makes the process of rebar spacing measurement more challenging. The emphasis now shifts to using computer vision techniques to maximize the benefits of UASs in construction projects.

This study introduces a semi-automated rebar inspection system that integrates low-cost RGBD camera with UAS technology, specifically optimized for real-world construction environments. This study contributes to the state-of-the-art in these ways: (1) system-level integration for field deployment beyond laboratory settings; (2) methodological optimization through systematic testing that identified optimal flight parameters (3 ft distance, horizontal movement) addressing construction-specific challenges; (3) combining 2D and 3D techniques on single-frame point cloud data, eliminating complex registration while achieving high accuracy (0.44 mm in field conditions); and (4) demonstration that commodity components can have high accuracy, improving accessibility for industry. This study showed a solution that helps inspector at elevated positions, improving safety and efficiency compared to traditional methods validated at an active construction site. This research explored the use of an RGBD-equipped UAS system through three different flight patterns and distances in a controlled setting, to identify the optimal parameters for data collection with UAS that yield the highest data quality in the context of rebar spacing measurements. We applied the result from the controlled environment setting on real construction sites on vertical rebar. Also, the proposed method combines 2D and 3D analytic techniques applied to point cloud data produced from a single frame using combination of the Hough transformation and Sobel edge detection algorithm. This combination effectively detect rebar edges in the scene. The output provides the results with different colors tailored to spacing errors, assisting inspector's understanding and enabling their decision on real-time.

3. Methodology

This section describes the approach used to estimate rebar spacing from point cloud data collected by RGBD-equipped UAS system. In the next sections, the rebar spacing measurement is detailed, with an emphasis on UAS utilization. Additionally, the integration of Sobel edge detection and the Hough transformation applied to a single frame is described.

3.1. Rebar spacing estimation workflow

The presented methodology introduces an automated system for collecting rebar data using RGBD-equipped UAS. We design a simplified experiment in controlled environments to find the optimal distance and flight pattern for UAS applications on construction site. The process begins with determining the UAS's optimal distance from the horizontal rebar. The primary reason for choosing a horizontal rebar mat is its widespread use in construction as a base material for construction and foundation installation. It provides a flat, uniform surface that is perfect for preliminary testing. This is followed by establishing a flight pattern, adjusting the camera parameters for ideal image capture, and selecting the most representative frames for data analysis.

Expanding on the results of the controlled experiment, the approach and system have been further validated by using them on a vertical rebar at a real construction site. This is done to evaluate the effectiveness of the method in an environment that is more dynamic and real-world than controlled, where factors like lighting, accessibility, and environmental conditions differ greatly. The objective of this experiment is to determine if the precision and reliability of the measurements, which had been previously observed, could be maintained during the shift from a horizontal rebar mat in a controlled environment to a vertical rebar arrangement in situ. In uncontrolled environments, the method adapts to vertical rebar by identifying the optimum distance for the UAS to maintain, the best flight pattern to cover the area effectively, and adjusting camera parameters to account for environmental variables all of which are obtained from the experience in the controlled environment. Safety considerations are important in these settings to protect the equipment and site.

The key performance indicators in this methodology are point cloud density, point spatial distribution, point cloud accuracy, and maximum coverage. These indicators were chosen to ensure high-quality data collection, and their importance is emphasized throughout the process. Both environments utilize a consistent analytical approach post-data acquisition including converting the data into a 2D raster projection, employing Sobel edge detection and Hough transformation to determine intersection points, and measuring spacing. Fig. 1 shows the workflow of the rebar spacing estimation using RGBD-equipped UAS.

3.2. Sobel edge detection and hough transformation

The developed algorithm in this study focuses on using a single frame rather than registering every frame. The underlying idea of this approach is that effective processing of a single frame can yield enough information to reliably detect rebar. In the context of rebar identification, two main assumptions have been considered for computer vision algorithm which are: (1) rebar is linear, and (2) rebar diameter is constant along their length. Hence, as long as the algorithm can fit a line with accuracy to the bars, it should be able to calculate the distance

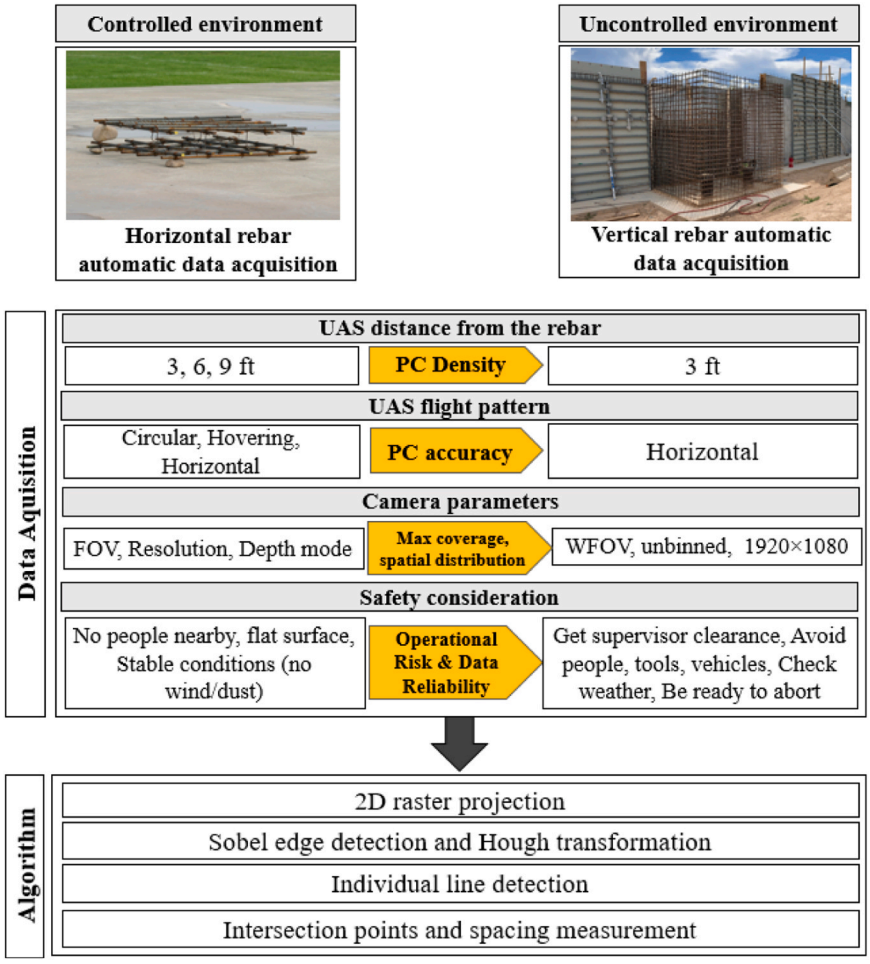

Fig. 1. Workflow of rebar spacing estimation using RGBD-equipped UAS.

between rebar. Methodology proposed in this paper combines 2D and 3D analysis, where the preprocessing will be done on 3D point cloud data of single frame and then further that frame will be converted into a 2D raster image (Fiume, 2014) for spacing measurement. In raster projection, points are transformed to a common coordinate system, projected onto a plane, and then mapped onto a grid. The resulting raster image represents a flattened representation of the original 3D point cloud data, with each pixel corresponding to a projected point. This step allows the application of conventional image-based analysis techniques to the point cloud data along with other 2D data sources.

To detect the individual lines for longitudinal and transverse rebar, the Sobel edge detection method (Braun and Borrmann, 2019) and Hough transformation (Argialas and Mavrantza, 2004) are combined. The Sobel operator enhances edge information to enable precise localization, and the Hough transform identifies lines based on the enhanced edges. Sobel edge detection uses the concept of spatial filters by applying two 3 × 3 convolution filters (one for the horizontal gradient (G_x) and one for the vertical gradient (G_y)) mentioned in Eq. (1).

$$G_x = \begin{bmatrix} -1 & 0 & 1 \\ -2 & 0 & 2 \\ -1 & 0 & 1 \end{bmatrix}, \quad G_y = \begin{bmatrix} -1 & -2 & 1 \\ 0 & 0 & 0 \\ 1 & 2 & 1 \end{bmatrix} \tag{1}$$

These kernels are convolved with the grayscale image to compute the gradient components at each pixel position (I,j) as mentioned in Eqs. (2) and (3).

$$G_x(i,j) = Image[i-1,\ j-1] + 2.\ Image[i,\ j-1] + Image[i+1,\ j-1] - Image[i-1,\ j+1] - 2.Image[i,\ j+1] - Image[i+1,\ j+1] \tag{2}$$

$$G_y(i,j) = Image[i-1,\ j-1] + 2.\ Image[i-1,\ j] + Image[i-1,\ j+1] - Image[i+1,\ j-1] - 2.Image[i+1,\ j] - Image[i+1,\ j+1] \tag{3}$$

The gradient magnitude is calculated using Eq. (4). Fig. 2 shows the result of the image after applying the Sobel edge detection.

$$GI = \sqrt{G_x I + I(i,j)^2} \tag{4}$$

For our implementation, we used an edge threshold value of 50, which was empirically determined to provide optimal edge detection for our rebar images while minimizing noise. As a result, regions with significant intensity changes corresponding to edges are highlighted in the resulting gradient magnitude image. The Hough transform is a feature extraction method that serves as an important tool for line detection in raster images. In doing so, the image space is transformed into a parameter space, which is often represented in the form of the slope-intercept of the linear equation. The Hough transformation converts each edge pixel (x, y) to a sinusoidal curve in the Hough parameter space (ρ, θ) in the form of the slope-intercept of the linear equation as mentioned in Eq. (5). Fig. 3 shows the transformation of edges in Hough space.

$$\rho = x \cos(\theta) + y \sin(\theta) \tag{5}$$

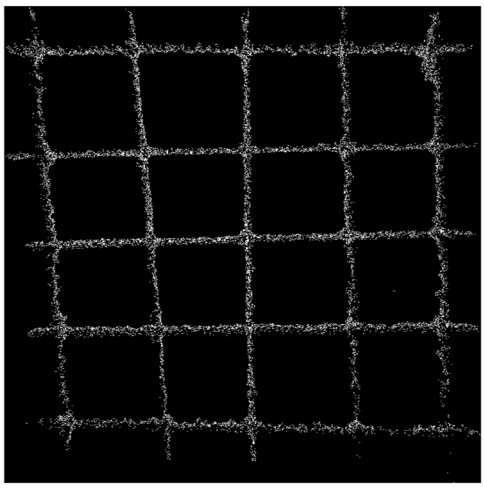

Fig. 2. Rebar mat after applying Sobel edge detection.

Each pixel in the image contributes multiple parameter values, resulting in a sine wave in Hough space. The intersection of these curves indicates the existence of lines in the original image. Finding peaks in Hough space can reliably identify lines and provide important parameters such as slope and intercept. We set the vote threshold to $H > 50$ for line confirmation, based on experimental results ensuring strong detection while avoiding false positives. We discretized ρ (distance from origin) with 1-pixel resolution and θ (angle) with 1° increments from -90° to 89°. The process begins by separating lines into horizontal and vertical categories based on their slope values, with a threshold of 10 serving as the classification criterion. This categorization is essential for distinguishing between longitudinal and transverse rebar in the grid structure. The algorithm then proceeds to calculate intersection points between horizontal and vertical lines by solving systems of linear equations, providing precise coordinates where rebar cross. These calculations yield the exact intersection points (x_intersect, y_intersect) using the determinant-based approach from analytical geometry. After identifying all potential intersection points, the algorithm verifies that each point lies within the actual line segments rather than their infinite extensions. The final phase implements a structured neighbor search with a radius of 200 pixels to identify adjacent intersection points. To prevent false neighbor associations, the algorithm applies filtering conditions that require minimum separations of 100 pixels in both x and y directions. The Euclidean distances between valid neighboring points are calculated and stored, providing direct measurements of rebar spacing that can be converted to real-world units using calibration data.

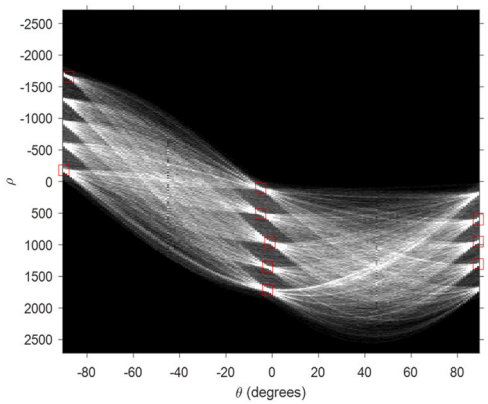

Fig. 3. Transformation of edges in Hough space.

4. Controlled outdoor experiment

This section summarizes a field test that was carried out on a horizontal rebar cage, at the Balloon Fiesta Park, New Mexico, to validate the applicability of the suggested rebar spacing approach. To replicate the real structural construction environment in the field, a two-layer rebar mat was built in the lab. The dimensions of the testbed were $27 \times 27 \times 9$ in^3 ($685.8 \times 685.8 \times 228.6$ mm^3). The dimensions of the rebar cage within the RC structure are 24 in (609.6 mm) in length, 24 in (609.6 mm) in width, and all bays for both layers of the #5 rebar have a spacing of 5 in (127 mm). The environmental conditions such as light and wind was normal. Data acquisition occurred over a 20-second period. Initially, three different distances – 3, 6, and 9 ft – as well as three different flight patterns - hovering, horizontal movement, and circular scanning - were selected to gather data for the analysis. This experiment enabled the researchers to find the best flight pattern and distance for further experiment. Fig. 4 shows the RGBD-equipped UAS system flying over the rebar mat.

4.1. Scanning device selection

The construction industry extensively utilizes 3D point cloud data for different applications such as inspection (Wang and Kim, 2019). Reconstruction of an object in three dimension and creating 3D point cloud data requires use of sensors such as LiDAR (Luo and Gavrilova, 2006). Table 3 presents six commonly used sensors and their attributes, including cost, accuracy, scanning scale, need for fixed reference points, environmental sensitivity, portability, real-time capability, and processing complexity. The researcher in this study used an inexpensive ($400) commodity RGBD camera: a Microsoft Azure Kinect, a third-generation Kinect featuring ToF technology for rebar inspection in the field because of its optimal balance of cost, portability, and ease of deployment. The RGBD camera is a low-cost alternative that provides sufficient accuracy for small to medium-scale inspections. RGBD camera can capture both color and depth data, allowing for rapid data collection, which is critical in dynamic construction environments. Additionally, it does not require fixed reference points or extensive setup, making it well-suited for use with UAS in active job sites. It may be moderately sensitive to lighting conditions, but its lightweight design and low data processing complexity make it a practical and efficient tool for automating rebar layout inspection in real-world construction scenarios.

The Azure Kinect RGBD camera provides multiple scanning modes and allows for optimization through the selection of different fields of view (FOV), operating ranges, and resolutions. This camera has 1-megapixel sensor for time-of-flight depth estimation. Furthermore, it features a 12-megapixel color camera. Due to safety concerns, the UAS kept at least approximately 3 ft from the rebar. Table 4 shows the selected mode of the camera for data collection. Based on the relevant properties and application in this study, we selected the FOV, resolution, and functional range of the camera for the data collection.

4.2. Hardware setup

The system developed for this project incorporated an advanced computer system, featuring a UAS equipped with Azure Kinect RGBD camera capabilities, enabling it to fly over the construction site and capture images of color and depth information simultaneously. This combination of RGBD sensors provided a comprehensive understanding of the construction site, enabling accurate 3D mapping and analysis. By using the aerial perspective provided by the UAS, the system can capture detailed data from different angles, heights, and is capable of covering a larger area efficiently. This system has three main parts: Azure Kinect camera, a power bank, and an onboard laptop. The Azure Kinect camera needed to be connected to a computer for data acquisition; therefore, to prevent safety issues, the 3D printed holder was specially designed and

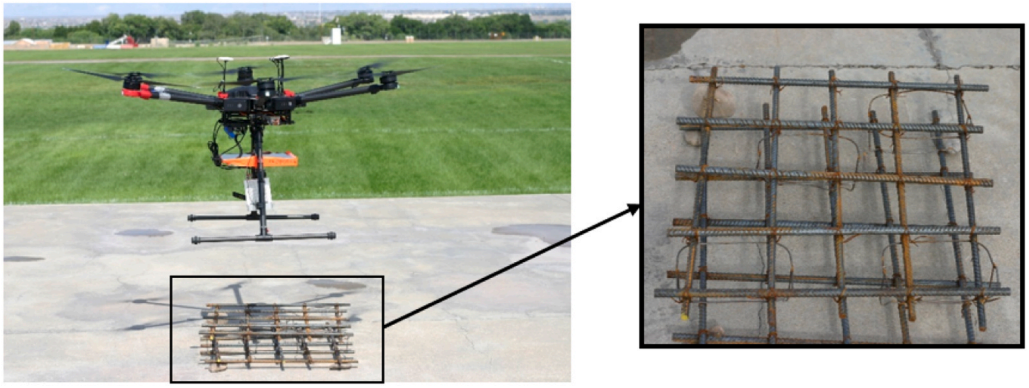

Fig. 4. RGBD-UAS and rebar mat.

Table 3
Comparison of sensor technologies for rebar inspection.

Sensor Type	Cost	Accuracy	Scanning area scale	Fixed points	Environmental sensitivity	Portability	Real-time?	Processing complexity
RGBD Camera	Low	Medium	Small–Medium	No	Moderate	High	Yes	Low–Moderate
LiDAR	High	High	Medium–Large	No	Low	Moderate	Yes	High
Structured Light	Medium	High	Small	Yes	High	Low	No	Moderate–High
ToF Sensor	Medium	Medium	Small–Medium	No	Moderate	High	Yes	Moderate
Ultrasonic Sensor	Low	Low	Small	Yes	Low	High	No	Low
Radar	High	Low–Medium	Medium–Large	No	Very Low	Moderate	No	High

Table 4
RGBD camera selected mode.

Properties	Value
Mode	Narrow-FOV unbinned
Field of View	75°× 65°
Resolution	640 × 576
Functioning range (m)	0.5–3.86
Frames Per Second (FPS)	30
Resolution (H×V)	1920 × 1080
Aspect Ratio	16:9
Format Options	MJPEG
Nominal FOV (HxV)	90°× 59°

manufactured to securely mount the onboard laptop to the UAS. An onboard power bank provided the power for the RGBD camera. Fig. 5 shows the overall configuration of the UAS used in the field experiment and 3D design of all the attached components.

4.3. Remote control system

The inspector used a remote system to control data acquisition. The system allowed the inspector to use another laptop to remotely access and control the onboard laptop connected to the RGBD camera. A secure and efficient remote connection was established between the two laptops using Team Viewer software (TeamViewer, n.d.), chosen for its security, ease of use, and cross-platform support. Team Viewer enabled the inspector to select a camera mode, start and stop data recording during flight. However, because TeamViewer's high resource usage may be an issue on some systems, other software might be preferable depending on available resources and system configuration. Alternative options include AnyDesk (The Fast Remote Desktop Application – AnyDesk, n.d.), which uses a codec to reduce CPU usage; Chrome

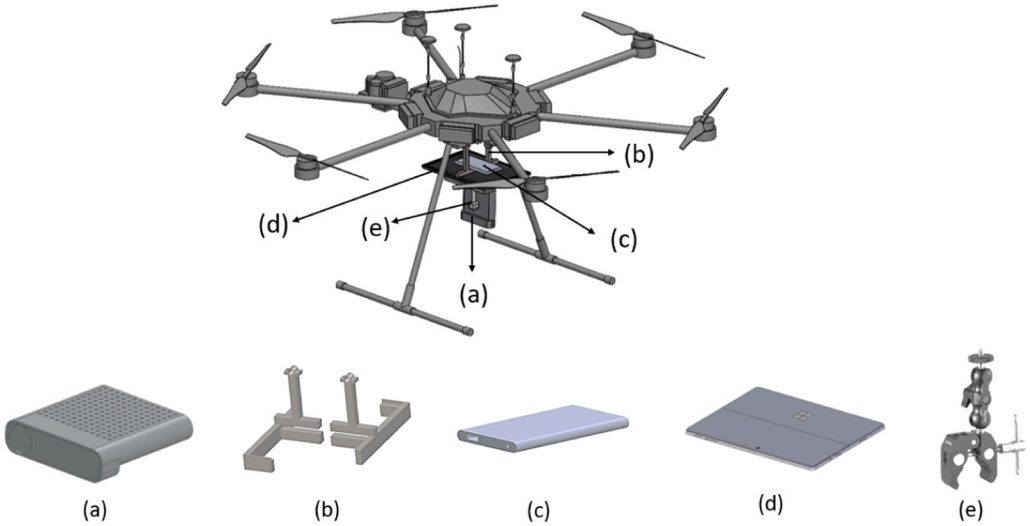

Fig. 5. Drone and installed equipment, (a) Azure Kinect camera, (b) laptop 3D printed holder, (c) power bank, (d) surface laptop, and (e) camera clamp.

Remote Desktop (Chrome Remote Desktop, n.d.), known for its simplicity and low resource consumption; and Microsoft Remote Desktop (Microsoft Store - Download Apps, Games and More for Your Windows PC, n.d.), which is a reliable option for Windows environments.

This remote-control system ensured seamless communication and allowed inspectors to actively participate in the data collection process, increasing the overall efficiency and convenience of the RGBD camera setup. For communication between the two laptops, a wireless network connection was established using hotspot. Fig. 6 shows the remote-control operation including the operator and laptops.

4.4. 3D point cloud data creation process

The process of analyzing 3D point cloud involves three main blocks as shown in Fig. 7. (1) creating 3D point cloud data starting with recording a video of the object (rebar) in.mkv format by selecting appropriate camera settings such as mode, FOV, resolution, recording time, and frame rate. Then the video is converted to a compatible format such as.ply or RGBD.png frames, which can be imported to software such as MATLAB or Cloud Compare for further analysis. (2) Pre-processing data which includes leveling the point cloud data, eliminating blurry or excessive points through noise reduction algorithms, down sampling and then doing the lens distortion based on the intrinsic parameters of the camera. (3) Analyzing the point cloud data through a raster projection, applying Sobel edge detection and Hough transformation techniques. This analysis enables the identification of both transverse and longitudinal rebar, allowing for subsequent spacing calculations. Details of the preprocessing and analysis will be explained in next sections.

4.5. Data preprocessing

Preprocessing the 3D point cloud includes four main steps: Leveling the point clouds to be parallel to xy-plane, noise reduction, down sampling, and dividing top and bottom layer of rebar.

During the leveling process, the point cloud is adjusted to align with the xy-plane. This is essential for eliminating any tilt or rotation that might have occurred during data collection. The leveling method used in this study involves fitting a plane to the point cloud data, using the robust estimator Maximum Likelihood Estimation Sample Consensus (MLESAC) (Torr and Zisserman, 2000), and adjusting the coordinates accordingly. MLESAC is an extension of the Random Sample Consensus (RANSAC) estimator (Schnabel et al., 2007), offering enhanced robustness in estimating model parameters. It takes a maximum likelihood estimation approach by iteratively selecting random subsets of data points and estimates the model parameters.

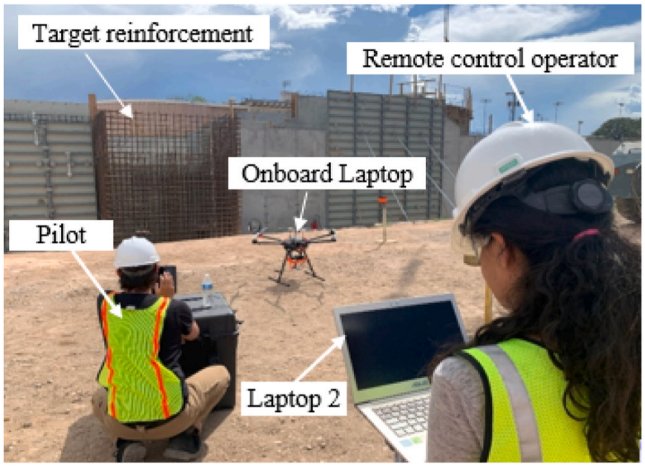

Fig. 6. Launch preparation.

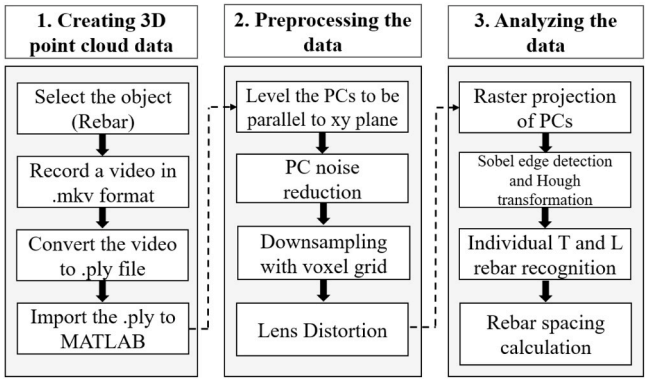

Fig. 7. 3D point cloud data creation, preprocessing, and analyzing steps.

The next step is noise reduction which is crucial for eliminating outliers in point cloud data. The technique used for noise reduction relies on finding the nearest neighbors of each point in the cloud and estimation of local surface properties (Rusu et al., 2008). Points that significantly deviate from the estimated surface are identified as noise and can be filtered out. However, such noise reduction techniques require parameter tuning by the user, including setting the number of nearest neighbors.

After that, down sampling is implemented to reduce the density of point cloud data by selecting a representative subset of points. This step is particularly useful for managing large and dense point clouds, as it reduces the computational and memory requirements for subsequent analysis. The voxel grid approach involves dividing the 3D space into small cubic cells (voxels), retaining only one representative point for each voxel, and discarding the rest (Pomerleau et al., 2013).

The final step in preprocessing is to divide the top and bottom layers of rebar. Z-coordinate histograms can be used as a valuable tool for splitting top and bottom layers based on observation of prominent peaks in the histograms. A careful analysis of the histogram can identify two distinct peaks corresponding to the top and bottom layers. The decisive factor for separation lies in the minimum between these peaks. This minimum represents the optimal threshold for effectively distinguishing layers. The selection of this threshold enables accurate subdivision of layers based on their z-coordinate values, facilitating efficient analysis and independent analysis of each layer. This pre-processing of the 3D point cloud data prepares the data for effective rebar separation analysis.

4.6. Results

The focus of this study was to capture a representative subset of the rebar (one frame). By adopting this approach, the integrity and quality of the results were consistently high, even when analyzing a single frame of data. This was achieved by enhancing the resolution and attention to detail within the specific region. In order to find the best parameters of UAS for further using it in field construction site, three different distances and flight pattern were tested in controlled environment as can be seen in Fig. 8.

Fig. 9 shows the captured point cloud data with the mentioned distance and flight patterns. As the drone hovered, it showed that precision decreased with height. At three feet, the coverage was dense, but it became sparser at six feet, showing only part of the ground and the shadow of the rebar mat, and quite sparse at nine feet. Drone movement was horizontal, and it showed that horizontal movement worked at lower altitudes because it kept a constant grid coverage at 3 feet, noticeable gaps at 6 feet, and a notable loss of pattern integrity at 9 feet. A comparable pattern could be seen in the circular scanning pattern, which started at 3 feet with a clearly defined grid and got less dense and

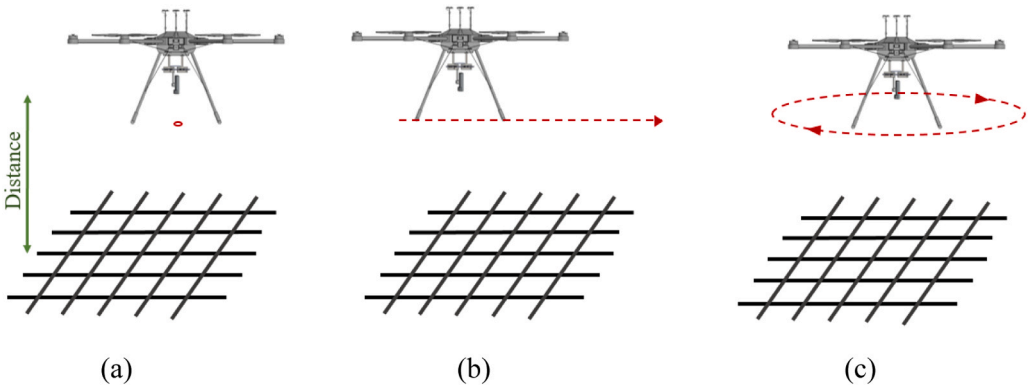

Fig. 8. UAS flight pattern; (a) Hovering, (b) Horizontal, and (c) Circular.

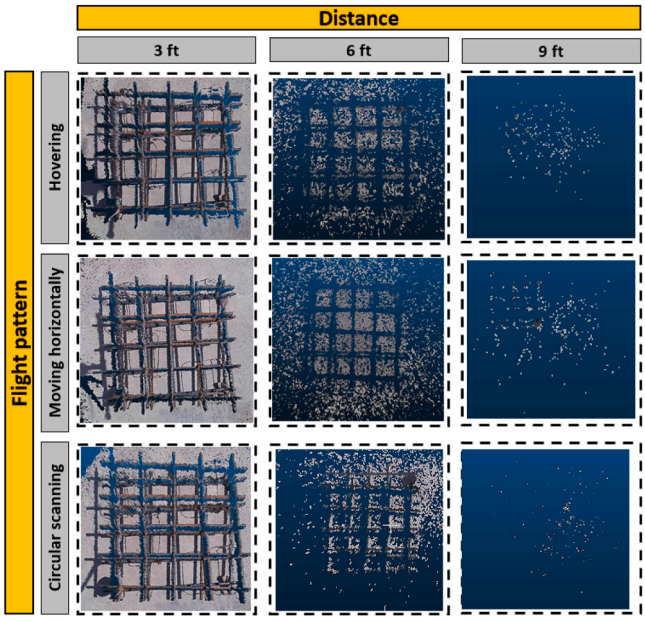

Fig. 9. RGBD-equipped UAS collected 3D point cloud at different distance and flight pattern.

more inconsistent as altitude rose, ending at 9 feet with minimum coverage. The effectiveness of collected data was affected by altitude, and this visual evaluation showed how crucial an ideal height was for attaining accurate area coverage. A comparison study of the various patterns at a height of three feet was carried out in order to determine the correlation between the accuracy of the rebar spacing measurement and drone flying patterns.

Fig. 10 shows the rebar mat and the 3D point cloud data created in this experiment, and line detection on one frame of rebar mat using the mentioned algorithm for moving horizontally flight pattern in 3 ft distance. The result is provided for top layer as an example. To validate the accuracy and applicability of the algorithm, the spacing of the rebar was measured using a steel tape and then compared with the spacing determined by the algorithm. The rebar spacing with tape was measured in the middle of each bay, rather than from corner point to point as depicted in Fig. 10(f).

To facilitate a comparison of spacing errors, the researcher averages the corner-to-corner spacing obtained from the algorithm to convert it into mid-bay spacing. Fig. 11 illustrates the conversion of corner-to-corner spacing into mid-bay spacing.

Fig. 11(a) shows the corner-to-corner distances calculated using the algorithm, where D_1, D_2 (horizontal distances) and D_3, D_4 (vertical distances) are measured from the middle line of the rebar at each intersection. These measurements show the actual detected distances but they are different from what inspectors typically measure. Fig. 11(b) shows how these values are converted into the mid-bay spacing used for inspection. Inspectors usually measure the center-to-center spacing between adjacent rebar rather than corner-to-corner distances. To align with this practice, the mid-bay horizontal spacing (D_H) is obtained by averaging D_1 and D_2, while the mid-bay vertical spacing (D_V) is calculated by averaging D_3 and D_4. This adjustment ensures that the algorithm's results are consistent with standard inspection methods for rebar spacing inspection.

Fig. 12 illustrates the difference in error in millimeters. Additionally, Table 5 presents the statistical parameters of the discrepancies between the spacing obtained by the algorithm and the tape measure, including horizontal and vertical spacing, along with their corresponding errors for all three flight patterns in 3 ft distance.

The statistical analysis of spacing error at a 3 ft distance shows that the "Horizontal movement" flight pattern offers the closest correlation with manual measurements, showing the smallest mean spacing difference. This pattern also shows the lowest percentage error, indicating a higher accuracy compared to the other methods. Although all three patterns—Hovering, Horizontal movement, and Circular scanning—show similar variability, as suggested by the nearly identical standard deviations, there are distinct variances in their precision and consistency. "Circular Scanning" has the highest percentage error, signifying lower accuracy. Despite these differences, the overall small magnitude of mean differences and standard deviations in millimeters shows a generally high level of precision across all flight patterns. Further experiments were carried out in a real-world construction setting to evaluate different rebar configurations and to explore real-world conditions. Based on this analysis, the "Horizontal movement" pattern was selected for field experiments conducted at a 3 ft distance. This experiment covered the complexities of field conditions and investigated another type of rebar mat, which was vertical reinforcement.

4.7. Time comparison of manual and automated rebar spacing

The time needed for inspection depends on the size of the scanned area, with each step taking a different amount of time. For a rebar specimen of size 2 by 2 ft used for controlled experiment, a manual spacing inspection was conducted by us in the field using a steel tape measure. The measured rebar spacing values of the top layer are shown in Fig. 13. A similar spacing measurement was also conducted for the bottom layer.

Table 6 provides an estimate of the time needed for each stage of the process using algorithm and manual measurement. These times represent the upper limit, as all the steps except for rebar scanning can be improved in the future to increase the efficiency of the algorithm. For

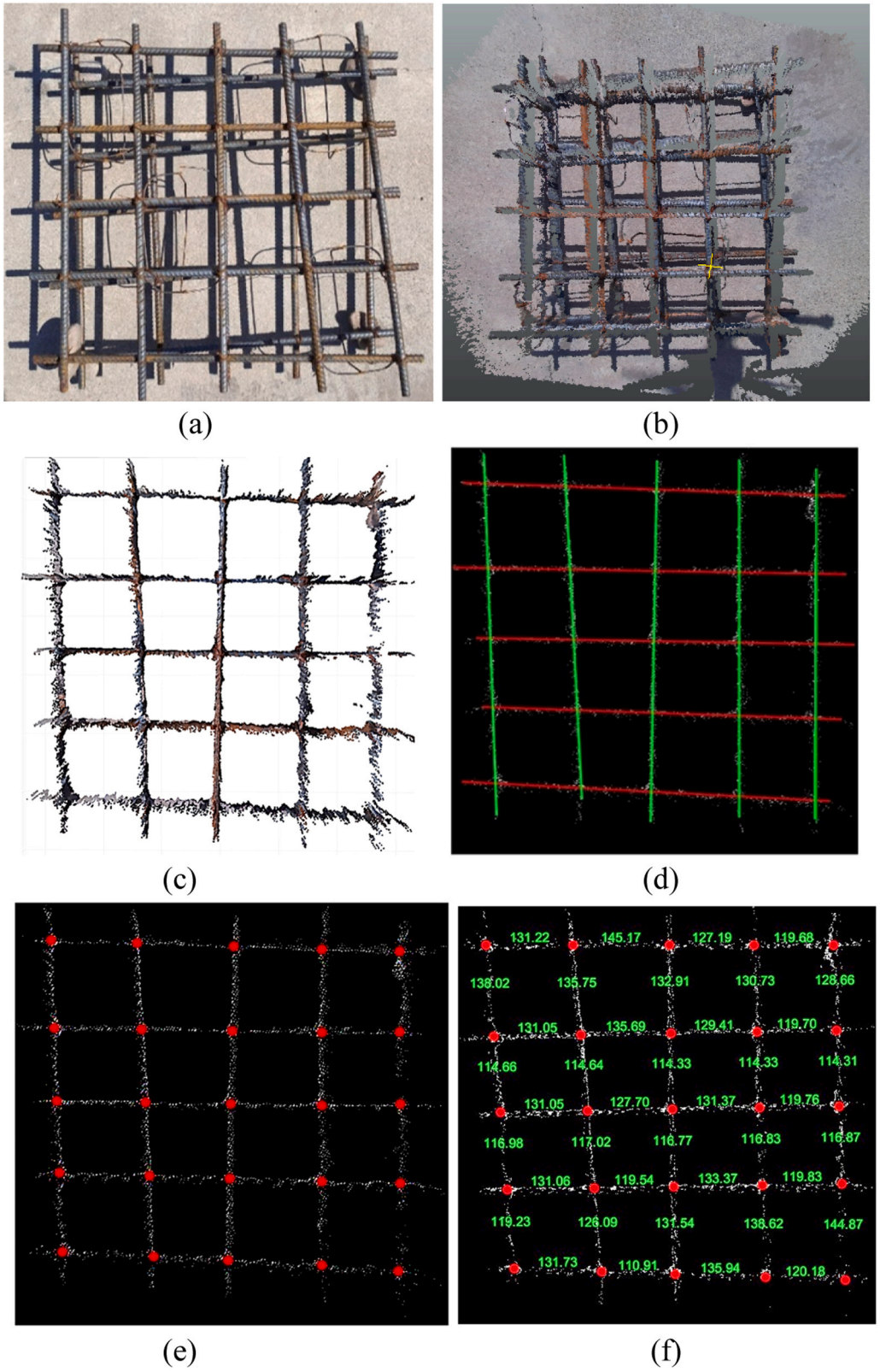

Fig. 10. 3D point cloud data creation, preprocessing, and analyzing; (a) photo of the rebar (b) original point cloud data, (c) top layer after preprocessing, (d) detected horizontal and vertical lines, (e) intersection points, and (f) algorithm spacing measurement.

the same specimen, the algorithm completed data collection and processing in 18 min and 27 s. The longest step in the process was generating the 3D point cloud data of the rebar, which is important as it directly impacts the accuracy of the results. For the spacing measurement of the bottom layer, the 3D point cloud data generation and preprocessing had already been implemented.

Table 7 presents projected time estimates for rebar inspection using manual methods versus the developed RGBD-UAS system across

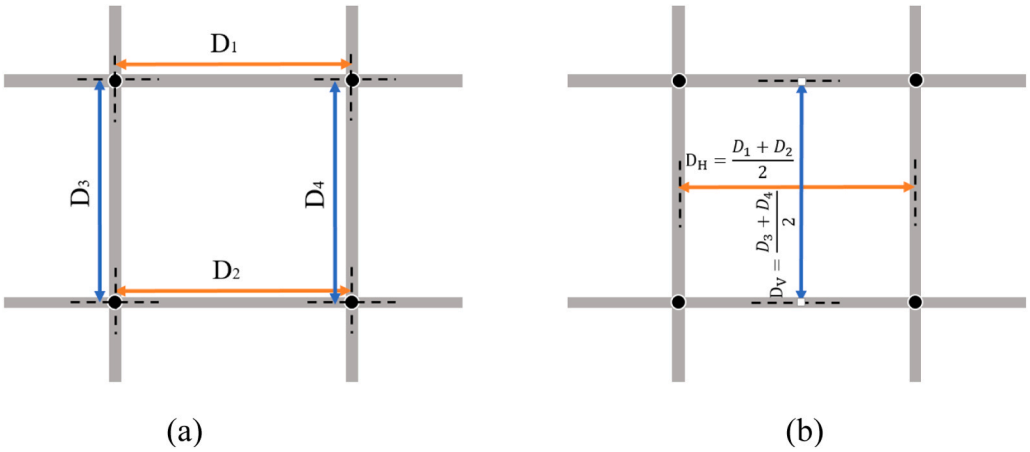

Fig. 11. Rebar spacing; (a) corner-to-corner spacing; (b) mid-bay spacing.

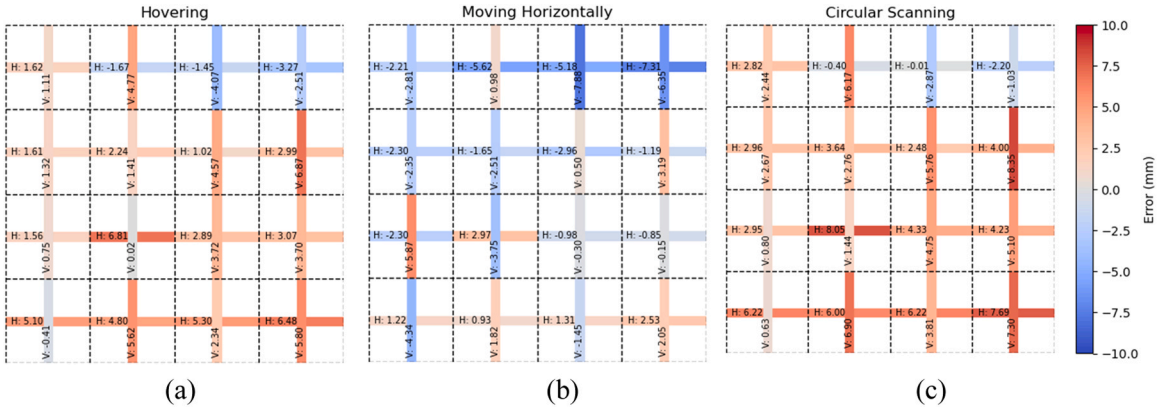

Fig. 12. Algorithm and tape measure rebar spacing error; (a) Hovering, (b) Moving horizontally, and (c) Circular scanning.

Table 5
Spacing difference statistical analysis for 3 ft distance.

	Hovering	Horizontal movement	Circular scanning
Mean (mm)	2.60	1.28	3.87
Standard deviation (mm)	3.14	3.13	3.10
Percentage error (%)	2.74	2.12	3.33

different site sizes. The updated comparative analysis shows the increasing efficiency of the RGBD-UAS approach as the inspection area increases. While manual inspection is slightly faster for very small areas such as a 2 × 2 ft section (14.5 min vs. 18.4 min), the advantages of automation become more apparent at larger scales. For example, inspecting a 20 × 50 ft area manually would take approximately 1376 min, compared to just 62.5 min using the RGBD-UAS system resulting in a time savings of over 95%. This trend continues with larger inspections: a 100 × 20 ft area requires 2752 min manually versus 124.8 min with automation, and a 500 × 40 ft inspection takes 27,503 min manually compared to only 623.5 min with the RGBD-UAS system. These projections assume a consistent experimental setup, matching the controlled 2 × 2 ft specimen in spacing and methodology. All manual inspections are performed by a single individual and include measuring spacing for both top and bottom rebar layers. This reflects realistic site conditions where inspectors must navigate horizontal rebar mats or elevated vertical configurations that demand physical effort, pose safety risks, and often lead to inconsistent measurements due to fatigue. In contrast, the RGBD-UAS system removes these physical burdens and supports uniform data collection regardless of site size or duration. However, field deployment of the RGBD-UAS system must consider practical limitations, such as drone battery life. A typical flight lasts around 15 min, after which batteries require replacement or recharging. This can result in an additional delay of 20–30 min depending on battery availability and logistics. The overall time savings achieved using this system at larger scales remain substantial and support the scalability and practical viability of the system in real-world construction scenarios.

5. Field experiment

To validate the proposed rebar spacing method using RGBD-equipped UAS, a field test was conducted at a construction site in White Rock, New Mexico, USA. The primary objective of this experiment was to validate the low-cost commodity RGBD methodology in an actual construction setting.

5.1. RC wall

According to the design drawing, the vertical wall rebar consists of #4 rebar spaced at 152.4 mm (6 in) in both longitudinal and transverse directions. The wall height is 4.4 m. Fig. 14 shows the plan view and isometric of the vertical reinforcement. The data is collected for 20 s in the Wide-FOV, unbinned camera mode with 1920 × 1080 resolution, and 30 fps. The drone made an ascending movement from bottom to top at a distance of 3 ft from the vertical wall. Fig. 15 shows the vertical wall reinforcement being used for inspection.

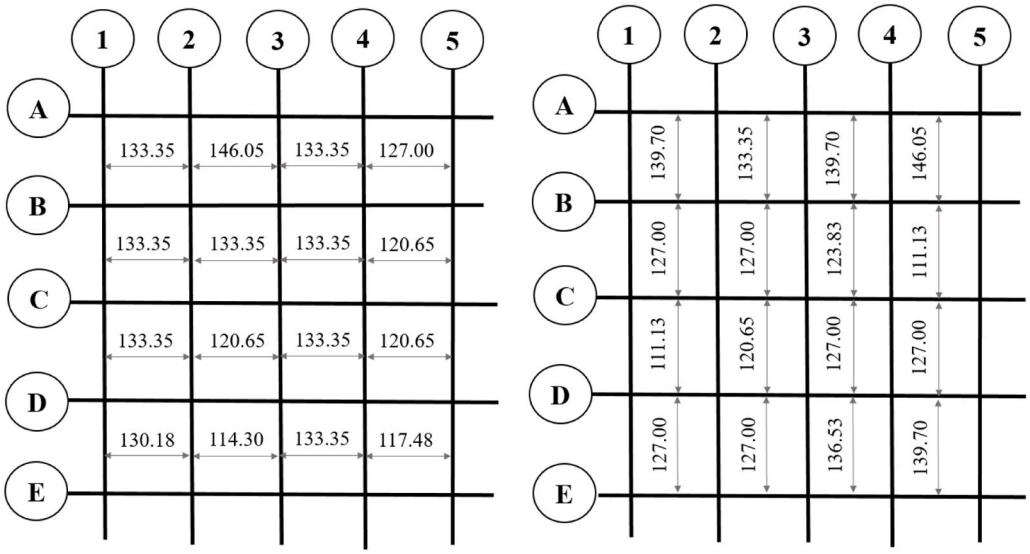

Fig. 13. Measured rebar top layer spacing using steel tape measure recorded in the field.

Table 6
Estimated time for different processing stages of controlled specimen rebar mat.

Processing stage	Duration (hh:mm:ss)	
	Automated inspection	Manual inspection
Rebar scanning	00:00:20	-
Creating 3D point cloud data	00:08:32	-
Preprocessing the point cloud	00:04:15	-
Spacing measurement – top layer	00:02:40	00:06:38
Spacing measurement – bottom layer	00:02:40	00:07:51
Total	00:18:27	00:14:29

5.2. Results and discussion

In this section all the preprocessing and processing analysis will be shown in detail. Fig. 16 shows the camera view for one frame out of 600 frames. The 3D point cloud data of part of vertical wall rebar consists of 677,997 points.

After importing the.ply file into MATLAB, the next step is to align the point cloud data to the xy-plane. This is because the orientation of rebar in 3D space can vary due to design tolerances, installation errors, or other factors. Aligning rebar data to the xy-plane creates a standardized frame of reference that allows for consistent measurements and comparisons. One approach to achieving this alignment is to fit a plane to the rebar point cloud and determine the angle between that plane and the xy-plane. This angle provides the information necessary to rotate the rebar data to place it in a horizontal position, ensuring accurate representations and facilitating further analysis and design decisions. Fig. 17 shows the rebar point cloud data, the plane that is fitted to it, and the rebar after alignment to the XY plane.

To perform the translation, it is important to note that the plane represented by the equation $ax+by+cz=d$ intersects the z-axis at the point $(0,\ 0,\ -d/c)$. By applying the translation vector $\vec{t}: (x,y,z)\rightarrow (x,y,z-d/c)$, a new plane $ax+by+cz=0$ is obtained that passes through the origin and is perpendicular to the vector $\vec{v}=(a,b,c)^T$.

Regarding the rotation, the angle between $\vec{v}$ and $\vec{k}=(0,\ 0,\ 1)^T$named as θ can be calculated using the Eq. (6).

$$\cos\theta = \frac{(\vec{v},\vec{k})}{|\vec{v}|} = \frac{c}{\sqrt{a^2+b^2+c^2}} \tag{6}$$

where a, b and c are the multipliers of the plane equation. The axis of rotation must be orthogonal to both $\vec{v}$ and $\vec{k}$, so its unit vector $(\hat{u})$ can be determined accordingly using Eq. (7). Eventually, the rotation matrix (α) can be represented by Eq. (8).

$$\hat{u} = \frac{\vec{v}\times\vec{k}}{|\vec{v}\times\vec{k}|} = \frac{1}{\sqrt{a^2+b^2}}(b,\ \ a,\ \ 0)^T = (u_1,\ \ u_2,\ \ 0)^T \tag{7}$$

$$\alpha = \begin{pmatrix} \cos\theta+{u_1}^2(1-\cos\theta) & u_1u_2(1-\cos\theta) & +u_2\sin\theta \\ u_1u_2(1-\cos\theta) & \cos\theta+{u_2}^2(1-\cos\theta) & -u_1\sin\theta \\ -u_2\sin\theta & +u_1\sin\theta & \cos\theta \end{pmatrix} \tag{8}$$

Noise in the point cloud is reduced by combing nearest neighbors. The number of nearest neighbors in this study were selected by experimenting with different neighborhood sizes and evaluating the noise reduction results. Noise in the point cloud is reduced using a data quality control process, where different neighborhood sizes are tested and evaluated using quantitative metrics such as noise reduction effectiveness, key feature retention, and overall smoothness. A visual check is

Table 7
Manual and RGBD-UAS inspection time projection.

Size	Manual Inspection			RGBD-UAS Inspection				Total Manual (min)	Total RGBD-UAS (min)
(ft × ft)	(min)			(min)					
	Setup	Measure	Doc	Scan	Cloud	Preproc	Measure		
2 × 2	1	8.5	5	0.3	8.5	4.3	5.3	14.5	18.4
20 × 50	1	1062.5	312.5	2	28.4	14.4	17.7	1376	62.5
100 × 20	2	2125	625	4	56.7	28.7	35.4	2752	124.8
300 × 30	2	9562.5	2812.5	12	170	86	106	12377	374
500 × 40	3	21250	6250	20	283.4	143.4	176.7	27503	623.5

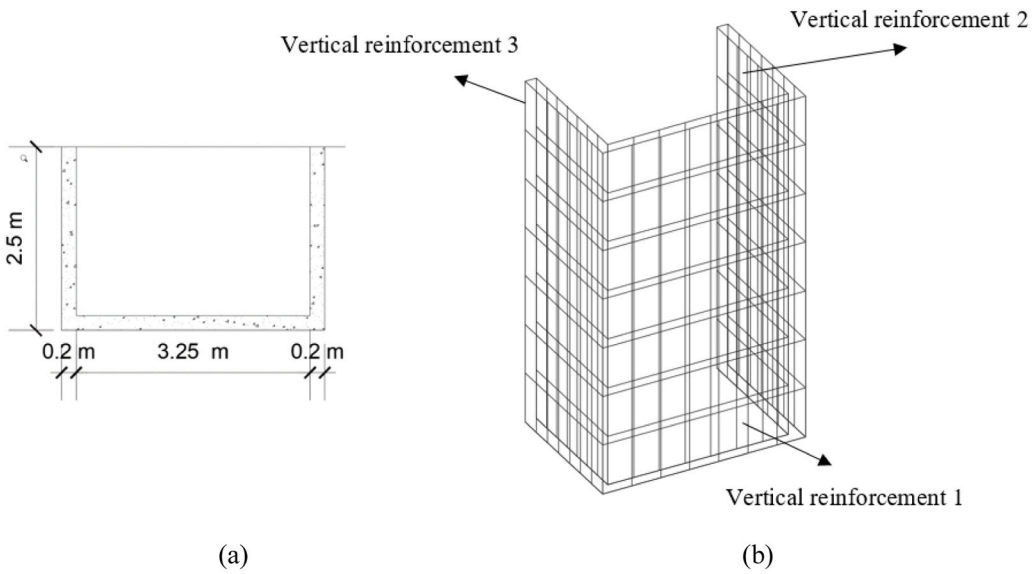

Fig. 14. Wall view (a) plan view, (b) isometric view.

Fig. 15. UAS-RGBD data collection at the construction site, White Rock, New Mexico.

conducted only after selecting the best-performing parameters to ensure that critical structural details are not lost or distorted. This final check is necessary because while numerical metrics guide optimization, they may not always detect small but important geometric features. This method improves accuracy by systematically selecting the optimal neighborhood size while reducing human subjectivity. However, the need for a final visual confirmation introduces a minor manual step, which could be further minimized in future work by fully automating denoising step. Based on these evaluations, a neighborhood size of 120 was selected which worked well empirically. There were 677,997 points in the original point cloud. The noise reduction procedure filtered approximately 5.50% of the data.

To find the best split point between the top and bottom layers of rebar, the lens distortion is implemented to eliminate the deviation from the expected geometry and avoid systematic errors. Then, two planes are fitted on the level of the two peaks in the z-histogram. A z-histogram plots the distribution of points along the z-axis. Since the point cloud data is parallel to the xy-plane, by identifying peaks corresponding to areas with the highest concentration of points, the spacing between layers can be approximated. Fig. 18 shows the two peaks in the z-histogram and the top and bottom layer of rebar correspond to each peak.

Fitting two planes to this peak allows accurate delineation of the top and bottom layers. This technique exploits the statistical properties of point cloud data and enables reliable determination of separation points, facilitating subsequent analysis and processing of rebar structures. Fig. 19 shows the two fitted plane on the z level according to z-histogram peaks. The green and red planes are fitted to top and bottom layer, respectively.

As previously described, preprocessing started with projection of point cloud data onto the 2D plane. Depending on the density of the data, desired level of detail, and computational resources for processing and storing an appropriate pixel size can be selected. In this example, a pixel size of 1 is selected for projection. Fig. 20 shows the rasterized

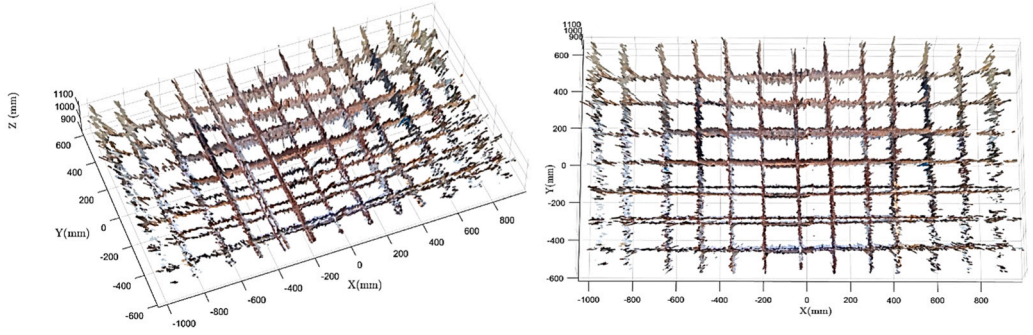

Fig. 16. Original point cloud.ply format: (a) 3D view, (b) xy view.

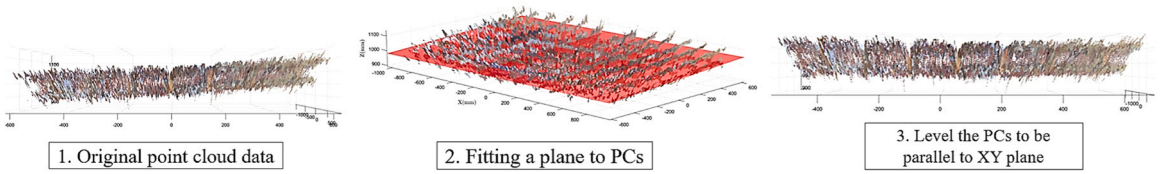

Fig. 17. Leveling the point cloud data to XY plane.

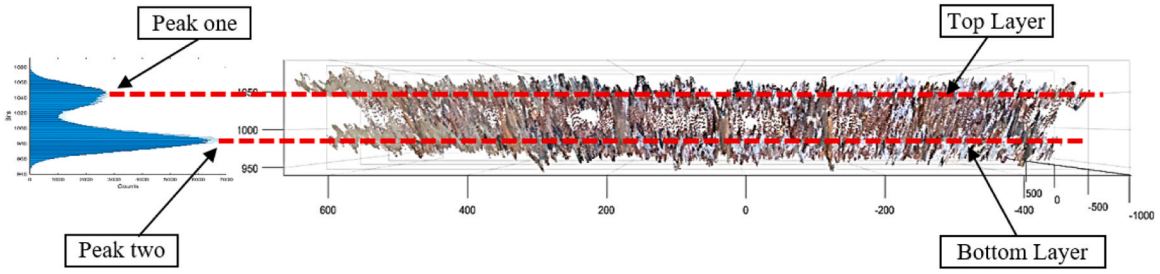

Fig. 18. Histogram, top and bottom rebar layer division.

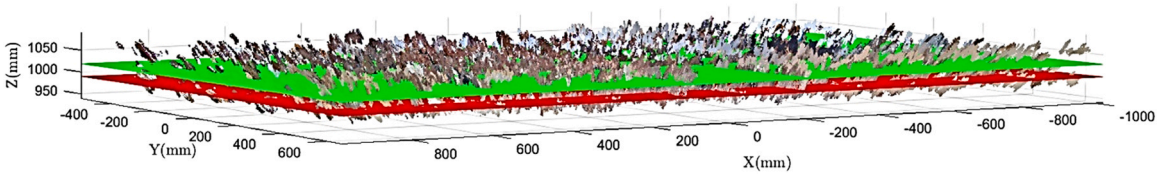

Fig. 19. Fitted plane to top and bottom layer on the z level of peaks at z-histogram.

projection of the top layer of the rebar. The selected subset is strategically chosen to provide meaningful insights into the rebar`s characteristics. By registering all frames, a comprehensive 3D point cloud data of the rebar can be generated.

Two important assumptions are made about rebar properties: (1) each rebar must be straight and (2) rebar diameter must remain constant over its length. These assumptions are used to simplify our calculations and help in the design process. These assumptions reflect an idealized scenario but provide a starting point for analysis and design. Actual variations and real-world imperfections can be accommodated by including appropriate margins of error. After raster projection of the point cloud data, Sobel edge detection algorithm and Hough transformation are employed to extract the horizontal and vertical lines for individual rebar. To start, Sobel edge detection algorithm is used to improve the edges by determining the gradient's amplitude and direction. The edges of the lines are highlighted by this step. The gradient magnitudes are then transformed into binary values during a thresholding process, which extracts important edge information while minimizing noise. The resulting binary edge picture is then subjected to the Hough transformation, which converts it into a parameter space with peaks standing for lines.

Information about the lines in the image is contained in the accumulator matrix produced by the Hough transformation. The parameters of these lines can be found by looking at the accumulator matrix and spotting the peaks. Finally, using the parameter values acquired from the Hough space, the lines are recovered from the original image as can be seen in Fig. 21. This figure also shows the vertical and horizontal rebar intersection points.

The gap between two consecutive lines in this algorithm is determined by the FillGap parameter of the 'houghlines' function in MATLAB. The code sets the FillGap value to 180. This means that the two line segments detected by the Hough transform are joined into one line within 180 pixels of each other. This parameter controls the maximum allowable gap between segments considered part of the same line.

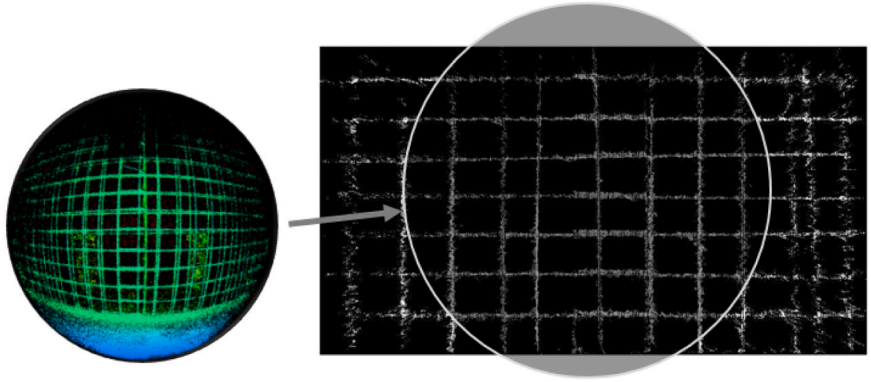

Fig. 20. Camera FOV for one frame.

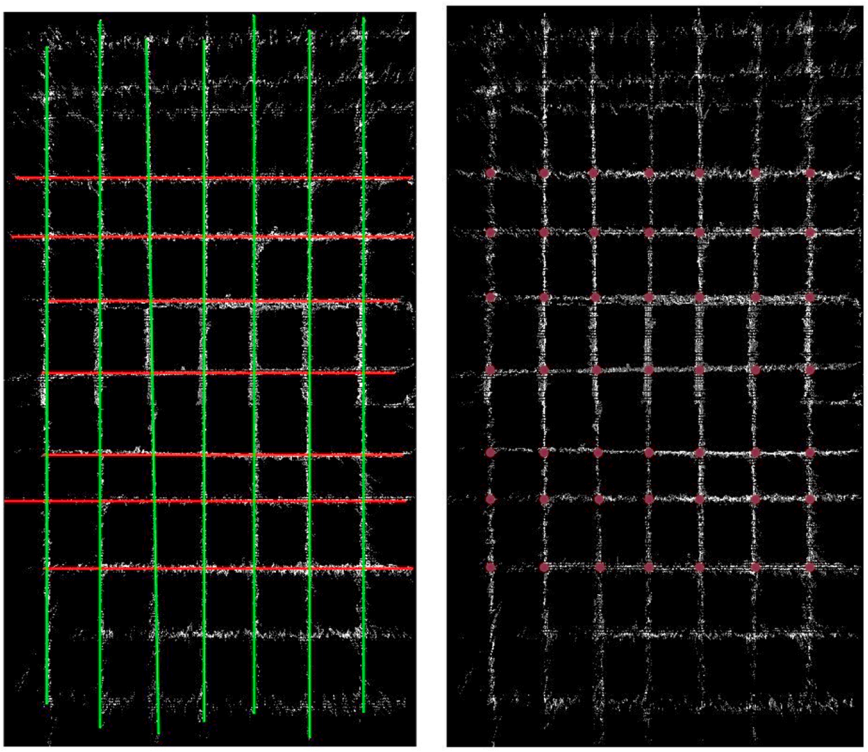

Fig. 21. (a) Detected horizontal and vertical rebar, (b) Extracted intersection points of horizontal and vertical rebar.

The next step is to find all the intersection points from horizontal and vertical lines and estimate the spacing by finding the distance between two points. Fig. 22 shows the spacing between all the neighbor points around each intersection in millimeters.

The proposed approach reduces the need for manual inspection, however, several steps in the workflow still depend on human input or empirically determined parameters. For example, visual validation currently follows algorithmic denoising; the optimal neighborhood size (120) was selected through empirical testing. Standardizing many of these parameters across similar inspection types can reduce the frequency of manual calibration. Once optimized for a given rebar configuration, settings such as neighborhood size for denoising, FillGap values for line detection, and edge detection thresholds can be consistently applied to future inspections involving similar structural layouts. Such standardization enhances repeatability while maintaining inspection accuracy. To achieve full automation, several improvements can replace remaining manual steps with algorithmic alternatives. An automated quality assessment framework for denoising can use quantitative indicators such as local surface variation percentages below 2%, consistent point density, and high feature retention scores to eliminate the need for visual inspection. Adaptive algorithms can determine optimal neighborhood sizes based on average point spacing multipliers and localized geometric complexity. For line detection, the Hough transformation parameters can be optimized iteratively to maximize detection accuracy while minimizing false positives, using accuracy thresholds above 95% as stopping criteria. These enhancements support consistent, objective, and scalable performance in alignment with the goals of a fully automated inspection system.

This study considered two types of errors in rebar spacing. The first error, shown in Fig. 23, is the difference between the spacing detected by the algorithm and the design drawings, which specify 6 in. (152.4 mm) horizontal and vertical spacing. These differences can be expressed in two ways: (1) The difference between the measured rebar spacing and the design drawing value represented in percentage error, (2) The difference between algorithm calculated spacing and the expected design spacing using color. The variance percentage serves as a quantitative indicator and provides information about the degree of deviation from design specifications. Additionally, color-coded distinctions allow for quick visual assessment, helping inspectors and engineers identify areas that require immediate attention or need further analysis.

However, construction does not always match the design due to inherent construction and human error, leading to the second error in Table 8. This error represents the difference between the spacing detected by the algorithm and the actual measurements in the field. There is always some level of error in construction, but as long as the deviations remain within the acceptable range, there is no issue in proceeding with the construction.

A specific bay was randomly selected to validate the accuracy of the proposed method. Horizontal and vertical spacing measurements were taken using a steel tape, providing a benchmark for comparison. Fig. 24 shows the location of the chosen bay on the vertical reinforcement. Table 8 displays the algorithm validation results for an example of longitudinal and transverse rebar spacing measurement. It compares the spacing measurement values obtained from the algorithm with those measured manually using a steel tape, which represents the actual constructed spacing in the field. The error is calculated as the absolute difference between these two measurements, expressed in both millimeters and percentage form. The formulas to obtain the error in mm and percentage is presented in Eq. (9), and Eq. (10) respectively.

$$\text{Error (mm)} = |\text{Actual measurement (construction)} - \text{Algorithm measurement}| \tag{9}$$

$$\text{Error}(\%) = \left(\frac{\text{Error}(\text{mm})}{\text{Actual measurement}(\text{construction})}\right) \times 100 \tag{10}$$

The horizontal spacing measured with the steel tape was 111.76 mm, while the vertical spacing measured 142.24 mm. According to the algorithm, the horizontal and vertical spacing were calculated as 111.02 mm and 142.37 mm, respectively. Comparing the algorithmic

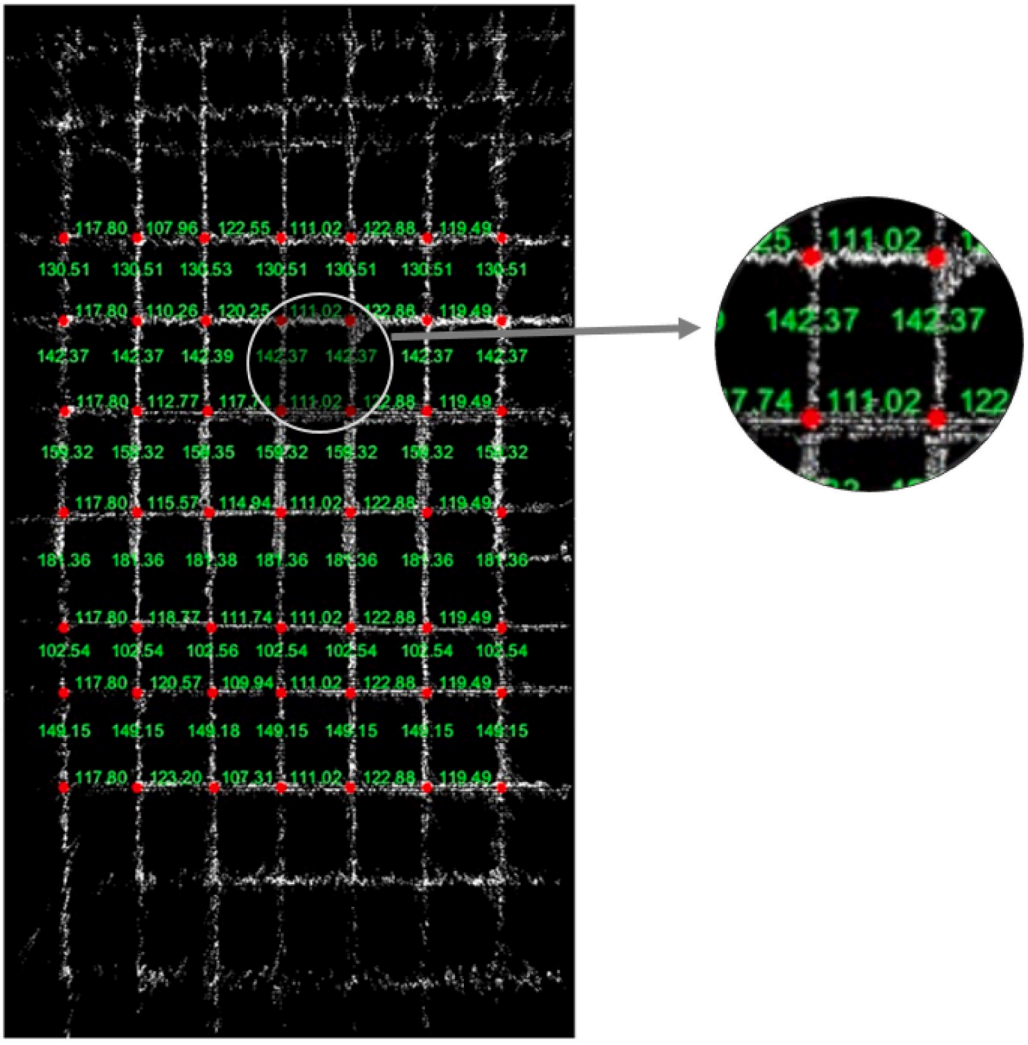

Fig. 22. Spacing between intersection points in millimeters.

estimates to the tape measurements, an average estimation error of 0.38% was observed which is equal to 0.44 mm. This difference suggests that the observed error within the rebar estimation context is within acceptable limits.

5.3. Comparative analysis

The section includes a comparison between the results of the present study and those from a related previous study that tested their rebar inspection algorithm in the real field. This analysis is intended to highlight how the current approach performs in relation to other recent methods for rebar inspection. Fig. 25 presents a radar chart comparing five field-tested rebar inspection methods across six key attributes: accuracy, efficiency, automation, robustness, cost, and scan time. The chart highlights the trade-offs each method makes to balance performance and practicality. For example, Wang et al. (2024) and Chang et al. (2024) demonstrated strong automation and accuracy, but their robustness is limited by high sensitivity to environmental variability. Owerko and Owerko (2021) provided high precision but suffers from low efficiency and high cost due to lengthy photogrammetry processing close to 48 h. Yuan et al. (2023) achieved rapid full-bridge inspection, but with limited automation and reliance on manual preprocessing and lower accuracy. The present study demonstrated a high accuracy, low cost, and fast processing particularly suited for field-deployable vertical rebar inspections. However, ongoing work is needed to improve its automation and environmental robustness to match the scalability of more complicated cases in construction site.

6. Automated RGBD-UAS data acquisition recommendations and limitations

Several important specifications must be considered to ensure accurate and reliable results in construction industry, when capturing rebar data with the described UAS system. The following section divides this consideration into three parts: camera, UAS, and construction site.

6.1. Consideration for the camera

It is important to mount the camera securely on the UAS to minimize vibration and provide an unobstructed view of the bars. We designed a 3D printed holder to secure the camera against vibration. Height and resolution must be balanced to maintain image sharpness and minimize motion blur. Additionally, it is important to set the camera setting appropriately to capture images at the optimum resolution and frame rate given the UAS's processing power and storage capacity limitations. It should be noted that the operation range of the Azure Kinect camera is from 0.25 m to 5.46 m; however, to consider the safety issues in the construction site, the UAS should be at least 1 m away from the object. Proper calibration of the Azure Kinect camera must be performed prior to data collection so that lens distortion can be corrected and rebar

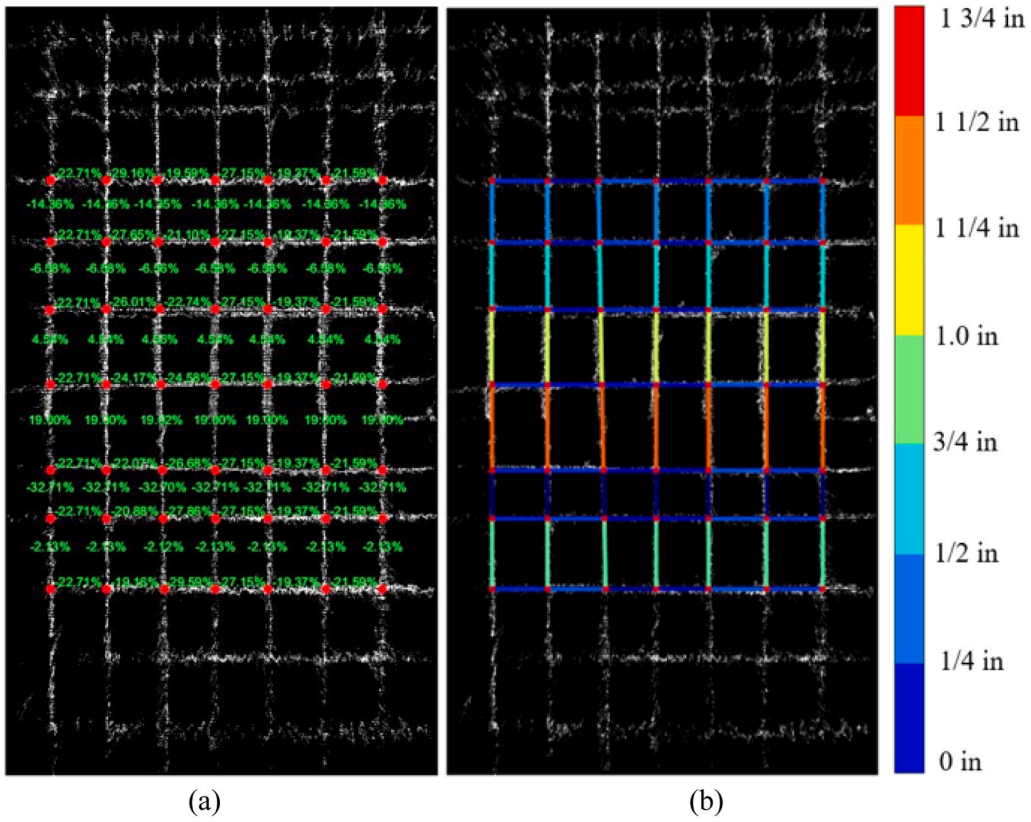

Fig. 23. Difference of algorithm calculated rebar spacing from expected design spacing (a) percentage representation, (b) color representation.

Table 8
Validation result.

Properties	Horizontal spacing (mm)	Vertical spacing (mm)
Steel tape	111.76	142.24
Algorithm	111.02	142.37
Error (mm)	0.74	0.13
Error (%)	0.66	0.09

dimensions and positions can be measured accurately. Storing RGBD camera data can be a challenge due to the large file sizes generated during recording. For example, a 20 s recording in.mkv format can result in a file size of approximately 1.2 GB, which can be computationally extensive when dealing with extensive 3D scans. To effectively manage.mkv data, it is important to consider having an external drive for transferring the data, especially in situations where large-area scans are required. Additionally, subsequent analysis must establish a safe and efficient method for transmitting data from the UAS to a specific storage location or processing unit.

Fig. 24. Vertical and horizontal spacing of rebar measured by the steel tape.

6.2. *Consideration for UAS*

The deployment of RGBD-equipped UAS for 3D point cloud data collection of rebar presents several technical and environmental challenges. Sensor limitations, including the shallow depth range of RGBD cameras, limit reliable detection of rebar embedded deep within structures or covered by overlapping materials. Environmental factors add to these challenges. Conditions like rain, fog, or intense sunlight can reduce sensor performance, and wind can affect both the stability of the flight and the quality of the data. Therefore, it is important to plan operations during favorable weather windows. Site-specific obstacles include dust contamination, which may require mitigation through ground watering or protective tarps. Magnetic interference from rebar can disrupt GPS signals, so maintaining

a minimum operational distance of 0.9–1.2 m can help to reduce this effect. Flight parameters require precise calibration: excessive altitude or velocity reduces resolution for thin rebar elements, whereas iterative testing confirmed that low-speed ascending movements yield optimal data fidelity. The current prototype faces additional constraints from its 3.9 lb payload (laptop and RGBD camera), which reduces flight duration to ~15 min and necessitates efficient trajectory planning. The custom 3D-printed mount reduces vibration, however a lightweight alternative using Raspberry Pi boards can help reduce payload by approximately 65% while maintaining processing capabilities. Future integration of Real-Time Kinematic (RTK) positioning could enhance navigation in

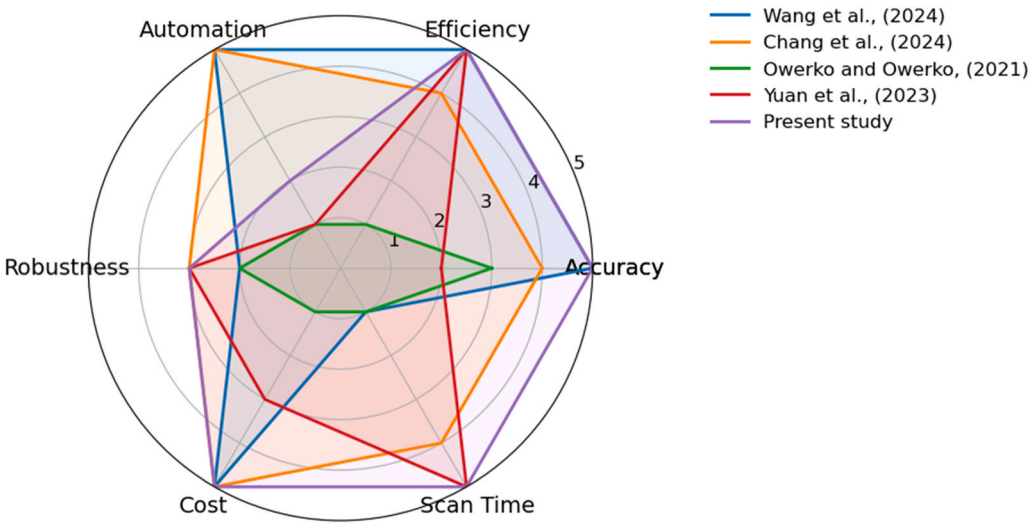

Fig. 25. Comparative analysis.

GPS-denied environments. These practical trade-offs highlight the need to balance sensor performance, flight stability, and adaptability to environmental conditions to ensure reliable use in the field.

6.3. Consideration in construction site

There are important considerations as well as opportunities for implementing the suggested RGBD-UAS system in active construction situations. It is essential to ensure UAS flight safety in accordance with local regulations, particularly on dynamic job sites where different lighting, weather changes, ongoing work, and physical clutter may impact both data quality and operational safety. For example, inspections conducted during active work hours may be interrupted by moving equipment, worker activity, or temporary obstructions. These issues can be minimized by scheduling scans during off-peak times. The use of RGBD camera provides some resilience to lighting variation, however, extreme sunlight or dust can reduce depth accuracy. In this case, the use of temporary shading or site dampening (e.g., watering the ground) is recommended. The system's modular and low-cost design enables deployment in a variety of structural contexts; however, real-world challenges such as rebar occlusion, irregular geometries, and tight spatial constraints may require additional planning, including optimized flight paths, orientation adjustments, and potentially scanning from different angles for complete coverage.

The system showed reliable performance under specific but representative conditions, primarily planar, grid-aligned, straight rebar configurations. These assumptions, explicitly incorporated into the computer vision algorithm to effectively detect rebar lines using a combination of Sobel edge detection and Hough transformation. The system's accuracy validated in both controlled lab and active field environments with spacing error as low as 0.44 mm. However, the current algorithm does not explicitly address complex geometries, bent or skewed bars, excessive site clutter, or significant occlusion.

Different enhancements are recommended to improve the system's application for more complex and less controlled settings: (1) Multi-frame registration or frame averaging to improve spatial completeness and reduce noise; (2) Multi-angle scanning to resolve occlusions and capture rebar from different views; (3) Machine learning-based detection, such as CNN, to adapt to irregular or partially occluded patterns; and (4) Sensor fusion to enhance reliability under poor lighting or high-clutter conditions.

7. Conclusion

Ensuring correct rebar spacing in RC structures is crucial for maintaining the structure's strength and durability. The traditional approach to rebar inspection is visual, which is subjective, time-consuming, and prone to safety issues. Recent technological advancements have motivated researchers to investigate automation in the RC construction industry using computer systems. This paper presented an automated method for field data acquisition for rebar spacing measurements using an RGBD-equipped UAS. Despite advances in cost-effective and accurate automatic rebar inspection methods that were investigated in previous research, many rely on high-quality data and stable conditions, limiting real-world applicability. To address these gaps, this study developed a low-cost data acquisition system using an RGBD-equipped UAS and computer vision technique suitable for both laboratory and construction site inspections. This method improves the accuracy of data collection. The developed algorithm integrates the Sobel edge detection and Hough transformation on 3D point cloud data collected by the system to extract all the lines correspond to rebar. Nine different experiments were conducted in controlled environment on horizontal rebar mat with 3, 6, and 9 ft distance, with hovering, one-way moving, and circular scanning flight pattern. The "One-way movement" flight pattern demonstrated the highest accuracy with the smallest mean difference and lowest error percentage in a 3 ft spacing analysis, making it the chosen method for field experiments focused on vertical reinforcement in construction settings. Then, functionality of this method was evaluated at a construction site in White Rock, New Mexico on a vertical rebar wall prior to concrete pouring based on the best distance and flight pattern obtained in controlled environment. The developed method showed an accuracy of 0.44 mm in construction site. For future research, several promising directions could be explored. The scalability and versatility of the proposed system can be studied by conducting experiments in different construction scenarios and evaluating its performance with different types of structures and reinforcement configurations. Additionally the potential to integrate AI-based decision support systems to automate the analysis of rebar spacing data and generate actionable insights promises increased construction efficiency and reduced errors.

CRediT authorship contribution statement

Fernando Moreu: Writing – review & editing, Visualization, Supervision, Resources, Project administration, Methodology, Investigation, Funding acquisition, Conceptualization. **Matthew G. Fricke:** Writing – review & editing, Visualization, Validation, Resources,

Conceptualization. **Ali Mohammadkhorasani:** Writing – review & editing, Visualization, Validation, Resources, Data curation. **Mahsa Sanei:** Writing – review & editing, Writing – original draft, Visualization, Validation, Supervision, Software, Resources, Methodology, Investigation, Formal analysis, Data curation, Conceptualization.

Declaration of Competing Interest

The authors declare that they have no known competing financial interests or personal relationships that could have appeared to influence the work reported in this paper.

Acknowledgment

The authors appreciate the support of Transportation Consortium of South-Central States (Tran-SET) for providing funding for this project (Grant No. 69A3551747106); NSF Division of Information & Intelligent Systems (IIS) CISE, Hardening the Data Revolution DSC, Grant/Award Number: 2123346; and Office of Naval Research, research program: Structural Reliability, ONR 331, Grant No: 13620990, Award Number: N00014–22–1–2638. The authors also acknowledge the support from the Department of Civil, Construction, and Environmental Engineering of the University of New Mexico (UNM); and the Center of Advanced Research and Computing (CARC) at UNM. The authors would also like to appreciate the help and assistance from Harry Chung, Morgan Merrill, and Gavin DeBerry.

Data availability

Data will be made available on request.

References

Argialas, Demetre P, Mavrantza, Ourania D, 2004. Comparison edge detection and hough transform techniques for the extraction of geologic features. Int. Arch. Photogramm. Remote Sens. Spat. Inf. Sci. 34, 790–795.

Asadi, Khashayar, Ramshankar, Hariharan, Pullagurla, Harish, et al., 2018. Vision-based integrated mobile robotic system for real-time applications in construction. Autom. Constr. 96 (December), 470–482. https://doi.org/10.1016/j.autcon.2018.10.009.

Braun, Alex, Borrmann, André, 2019. Combining inverse photogrammetry and BIM for automated labeling of construction site images for machine learning. Autom. Constr. 106 (October), 102879. https://doi.org/10.1016/j.autcon.2019.102879.

Chang, Chun-Cheng, Huang, Tsung-Wei, Chen, Yi-Hsiang, Lin, Jacob J., Chen, Chuin-Shan, 2024. Autonomous dimensional inspection and issue tracking of rebar using semantically enriched 3D models. Autom. Constr. 160 (April), 105303. https://doi.org/10.1016/j.autcon.2024.105303.

Chrome Remote Desktop. n.d. Accessed February 20, 2025. ⟨https://remotedesktop.google.com/?pli=1⟩.

Eschmann, Christian, Chen-Ming Kuo, Chung-Hsin Kuo, and Christian Boller. 2012. Unmanned Aircraft Systems for Remote Building Inspection and Monitoring. 13–14. ⟨https://www.researchgate.net/publication/279527780_Unmanned_Aircraft_Systems_for_Remote_Building_Inspection_and_Monitoring⟩.

Faria, Margarida, Ferreira, António Sérgio, Pérez-Leon, Héctor, Maza, Ivan, Viguria, Antidio, 2019. Autonomous 3D exploration of large structures using an UAV equipped with a 2D LIDAR. Sensors 19 (22), 22. https://doi.org/10.3390/s19224849.

Fiume, Eugene L., 2014. The mathematical structure of raster graphics. Academic Press.

Gaspari, F., Ioli, F., Barbieri, F., Belcore, E., Pinto, L., 2022. Integration of Uav-Lidar and Uav-photogrammetry for infrastructure monitoring and bridge assessment. ISPRS - Int. Arch. Photogramm. Remote Sens. Spat. Inf. Sci. 43B2 (May) 995–1002. https://doi.org/10.5194/isprs-archives-XLIII-B2-2022-995-2022.

Golparvar-Fard, Mani, Ghadimi, Behshad, Saidi, Kamel S., Cheok, Geraldine S., Franaszek, Marek, Lipman, Robert R., 2012. Image-based 3D mapping of rebar location for automated assessment of safe drilling areas prior to placing embedments in concrete bridge decks. July 11, 960–970. https://doi.org/10.1061/9780784412329.097.

Han, Kevin, JunYoung, Gwak, Mani, Golparvar-Fard, et al., 2013. Vision-based field inspection of concrete reinforcing bars. CONVR 2013.

Hill, Will, Jalloul, Hiba, Movahedi, Mohammad, Choi, Juyeong, 2023. Sustainable management of the built environment from the life cycle perspective. J. Manag. Eng. 39 (2), 03123001. https://doi.org/10.1061/JMENEA.MEENG-4759.

Jordan, Sophie, Moore, Julian, Hovet, Sierra, et al., 2018. State-of-the-art technologies for UAV inspections. IET Radar Sonar & Navig. 12 (2), 151–164. https://doi.org/10.1049/iet-rsn.2017.0251.

Jung, Sungwook, Song, Seungwon, Kim, Sanghyeon, et al., 2019. Toward autonomous bridge inspection: a framework and experimental results. 16th Int. Conf. Ubiquitous Robots (UR) 2019 (June), 208–211. https://doi.org/10.1109/URAI.2019.8768677.

Kim, Min-Koo, Thedja, Julian Pratama Putra, Wang, Qian, 2020. Automated dimensional quality assessment for formwork and rebar of reinforced concrete components using 3D point cloud data. Autom. Constr. 112 (April), 103077. https://doi.org/10.1016/j.autcon.2020.103077.

Kim, Min-Koo, Thedja, Julian Pratama Putra, Chi, Hung-Lin, Lee, Dong-Eun, 2021. Automated rebar diameter classification using point cloud data based machine learning. Autom. Constr. 122 (February), 103476. https://doi.org/10.1016/j.autcon.2020.103476.

Luo, Yuan, Gavrilova, Marina L., 2006. 3D building reconstruction from LIDAR data. Computational Science and Its Applications - ICCSA 2006. Lecture Notes in Computer Science, Berlin, Heidelberg, pp. 431–439. https://doi.org/10.1007/11751540_46.

Ma, Xiaocheng, He, Zongfeng, Xu, Ziqi, Wang, Wei, Xiao, Jian, 2022. Machine vision-based surface inspection system for rebar. In: 2022 IEEE 10th Joint International Information Technology and Artificial Intelligence Conference (ITAIC), 10, pp. 2634–2637. https://doi.org/10.1109/ITAIC54216.2022.9836480.

Marchisotti, Daniele, Zappa, Emanuele, 2022. Feasibility study of drone-based 3-D measurement of defects in concrete structures. IEEE Trans. Instrum. Meas. 71, 1–11.

Masoumi, F., Akgül, F., Mehrabzadeh, A., 2013. Condition assessment of reinforced concrete bridges by combined nondestructive test techniques. Int. J. Eng. Technol. 708–711. https://doi.org/10.7763/IJET.2013.V5.647.

Metni, Najib, Hamel, Tarek, 2007. A UAV for bridge inspection: visual servoing control law with orientation limits. Autom. Constr. 17 (1), 3–10. https://doi.org/10.1016/j.autcon.2006.12.010.

Microsoft Store - Download Apps, Games & More for Your Windows PC. n.d. Microsoft Remote Desktop - Free Download and Install on Windows | Microsoft Store. Accessed February 20, 2025. ⟨https://apps.microsoft.com/detail/9wzdncrfj3ps?hl=en-US&gl=US⟩.

Mohammadkhorasani, Ali, Malek, Kaveh, Mojidra, Rushil, et al., 2023. Augmented reality-computer vision combination for automatic fatigue crack detection and localization. Comput. Ind. 149, 103936.

Narasimhan, Sriram, Wang, Yang, 2020. Noncontact sensing technologies for bridge structural health assessment. J. Bridge Eng. 25 (6), 02020001. https://doi.org/10.1061/(ASCE)BE.1943-5592.0001560.

Nasrollahi, Majid, Bolourian, Neshat, Zhu, Zhenhua, Hammad, Amin, 2018. Designing LiDAR-equipped UAV platform for structural inspection. ISARC Proc. 1092–1099. July 22.

Nishio, Koji, Nakamura, Noriyoshi, Muraki, Yuta, Kobori, Ken-ichi, 2017. A method of core wire extraction from point cloud data of rebar. V. áclav Skala - UNION Agency. ⟨http://dspace5.zcu.cz/handle/11025/29734⟩.

Owerko, Piotr, Owerko, Tomasz, 2021. Novel approach to inspections of as-built reinforcement in incrementally launched bridges by means of computer vision-based point cloud data. IEEE Sens. J. 21 (10), 11822–11833. https://doi.org/10.1109/JSEN.2020.3020132.

Pantazopoulou, S.J., Papoulia, K.D., 2001. Modeling cover-cracking due to reinforcement corrosion in RC structures. J. Eng. Mech. 127 (4), 342–351. https://doi.org/10.1061/(ASCE)0733-9399(2001)127:4(342).

Ploennigs, Joern, Anika, Schumann, Freddy, Lécué, 2014. Adapting semantic sensor networks for smart building diagnosis. The Semantic Web – ISWC 2014, edited by Peter Mika, Tania Tudorache, Abraham Bernstein, et al. Lecture Notes in Computer Science. Springer International Publishing. https://doi.org/10.1007/978-3-319-11915-1_20.

Pomerleau, Francois, Colas, Francis, Siegwart, Roland, Magnenat, Stephane, 2013. Comparing ICP variants on real-world data sets. Auton. Robots (34), 133–148.

Qureshi, Abdul Hannan, Alaloul, Wesam Salah, Murtiyoso, Arnadi, Hussain, Syed Jawad, Saad, Syed, Musarat, Muhammad Ali, 2024. Smart rebar progress monitoring using 3d point cloud model. Expert Syst. Appl. 249 (September), 123562. https://doi.org/10.1016/j.eswa.2024.123562.

Roca, D., Armesto, J., Lagüela, S., Díaz-Vilariño, L., 2014. Lidar-equipped Uav for building information modelling. ISPRS - Int. Arch. Photogramm. Remote Sens. Spat. Inf. Sci. XL5 (June), 523–527. https://doi.org/10.5194/isprsarchives-XL-5-523-2014.

Rusu, Radu Bogdan, Marton, Zoltan Csaba, Blodow, Nico, Dolha, Mihai, Beetz, Michael, 2008. Towards 3D point cloud based object maps for household environments. In: Robotics and Autonomous Systems, 56. Semantic Knowledge in Robotics, pp. 927–941. https://doi.org/10.1016/j.robot.2008.08.005.

Sanei, Mahsa, Yuan, Xinxing, Moreu, Fernando, Alampalli, Sreenivas, 2023. Automated geometric quality inspection of rebar layout using RGBD data. Mater. Eval. 81 (1), 46–55. https://doi.org/10.32548/2023.me-04307.

Sanford, K.L., Herabat, P., McNeil, S., 1999. Bridge management and inspection data: leveraging the data and identifying the gaps. Paper presented at Eighth Transportation Research Board Conference on Bridge ManagementTransportation Research Board Committee on Bridge Maintenance and Management (A3C06). B-1, IBMC-061. B-1, IBMC-061. ⟨https://trid.trb.org/view/500539⟩.

Santos, R., Ribeiro, D., Lopes, P., Cabral, R., Calçada, R., 2022. Detection of exposed steel rebars based on deep-learning techniques and unmanned aerial vehicles. Autom. Constr. 139 (July), 104324. https://doi.org/10.1016/j.autcon.2022.104324.

Schnabel, R., Wahl, R., Klein, R., 2007. Efficient RANSAC for point-cloud shape detection. Comput. Graph. Forum 26 (2), 214–226. https://doi.org/10.1111/j.1467-8659.2007.01016.x.

Schwind, Michael A., Ralph, A.Scheid, Jonathan, L.Boone, 2018. A Comparative analysis of LiDAR and structure from motion photogrammetry utilizing a small unmanned aerial system (sUAS) approach for structural mapping and inspection. Report.

Information Technology Laboratory (U.S.). ⟨https://erdc-library.erdc.dren.mil/jspui/handle/11681/29513⟩.
TeamViewer. n.d. TeamViewer – The Remote Connectivity Software. Accessed December 27, 2023. ⟨https://www.teamviewer.com/en-us/⟩.
The Fast Remote Desktop Application – AnyDesk. n.d. Accessed February 20, 2025. ⟨https://anydesk.com/en⟩.
Torr, P.H.S., Zisserman, A., 2000. MLESAC: a new robust estimator with application to estimating image geometry. Comput. Vis. Image Underst. 78 (1), 138–156. https://doi.org/10.1006/cviu.1999.0832.
Villani, Valeria, Pini, Fabio, Leali, Francesco, Secchi, Cristian, 2018. Survey on human–robot collaboration in industrial settings: safety, intuitive interfaces and applications. Mechatronics 55 (December), 248–266. https://doi.org/10.1016/j.mechatronics.2018.02.009.
Wang, Dong, Gao, Lin, Zheng, Junxing, Xi, Junbo, Zhong, Jichen, 2025. Automated recognition and rebar dimensional assessment of prefabricated bridge components from low-cost 3D laser scanner. Measurement 242 (January), 115765. https://doi.org/10.1016/j.measurement.2024.115765.
Wang, Qian, Kim, Min-Koo, 2019. Applications of 3D point cloud data in the construction industry: a fifteen-year review from 2004 to 2018. Adv. Eng. Inform. 39 (January), 306–319. https://doi.org/10.1016/j.aei.2019.02.007.
Wang, Qian, Cheng, Jack C.P., Sohn, Hoon, 2017. Automated estimation of reinforced precast concrete rebar positions using colored laser scan data. Comput. -Aided Civ. Infrastruct. Eng. 32 (9), 787–802. https://doi.org/10.1111/mice.12293.
Wang, Seunghyeon, Kim, Mincheol, Hae, Hyeonyong, Cao, Mengqiu, Kim, Juhyung, 2023. The development of a rebar-counting model for reinforced concrete columns: using an unmanned aerial vehicle and deep-learning approach. J. Constr. Eng. Manag. 149 (11), 04023111. https://doi.org/10.1061/JCEMD4.COENG-13686.
Wang, Seunghyeon, Eum, Ikchul, Park, Sangkyun, Kim, Jaejun, 2024. A labelled dataset for rebar counting inspection on construction sites using unmanned aerial vehicles. Data Brief. 55 (August), 110720. https://doi.org/10.1016/j.dib.2024.110720.
Washer, Glenn A., and Alec Chang. 2009. *Guideline for Implementing Quality Control and Quality Assurance for Bridge Inspection*. National Cooperative Highway Research Program NCHRP Project 20-07. Task 252. University of Missouri–Columbia. https://doi.org/10.32469/10355/6560.
Wood, Richard L., Mitra Nasimi, Bowen Yang, et al. 2022. *Outdoor Laboratory and Testbed for Bridge Health*. M107. June, M107. ⟨https://trid.trb.org/view/2011953⟩.
Yuan, Xinxing, Smith, Alan, Sarlo, Rodrigo, Lippitt, Christopher D., Moreu, Fernando, 2021. Automatic evaluation of rebar spacing using LiDAR data. Autom. Constr. 131 (December), 103890. https://doi.org/10.1016/j.autcon.2021.103890.
Yuan, Xinxing, Moreu, Fernando, Hojati, Maryam, 2021. Cost-effective inspection of rebar spacing and clearance using RGB-D sensors. Sustainability 13 (22), 22. https://doi.org/10.3390/su132212509.
Yuan, Xinxing, Smith, Alan, Moreu, Fernando, et al., 2023. Automatic evaluation of rebar spacing and quality using LiDAR data: field application for bridge structural assessment. Autom. Constr. 146 (February), 104708. https://doi.org/10.1016/j.autcon.2022.104708.
Zhang, Xinman, Zhang, Jiayu, Ma, Mei, et al., 2018. A high precision quality inspection system for steel bars based on machine vision. Sens. (Basel Switz.) 18 (8), 2732. https://doi.org/10.3390/s18082732.

Glossary

AI: Artificial Intelligence
AP50: Average Precision at 50% Intersection over Union
BIM: Building Information Modeling
CNN: Convolutional Neural Networks
DBSCAN: Density-Based Spatial Clustering of Applications with Noise
DQA: Dimensional Quality Assessment
GMM: Gaussian Mixture Model
HDS: High Definition Surveying
MAE: Mean Absolute Error
ML: Machine Learning
MVS: Multi-View Stereo
OCC: Object-based Change Classification
PCA: Principal Component Analysis
RANSAC: Random Sample Consensus
R-CNN: Region-based Convolutional Neural Network
SfM: Structure from Motion
TLS: Terrestrial Laser Scanner
YOLO: You Only Look Once